Uniform Passive Fault-Tolerant Control of a Quadcopter with One, Two, or Three Rotor Failure

Chenxu Ke, Kai-Yuan Cai, and Quan Quan,

Abstract—This study proposes a uniform passive fault-tolerant control (FTC) method for a quadcopter that does not rely on fault information subject to one, two adjacent, two opposite, or three rotor failure. The uniform control implies that the passive FTC is able to cover the condition from quadcopter fault-free to rotor failure without the need for controller switching. To achieve the purpose of passive FTC, the rotors' fault is modeled as a lumped disturbance acting on the virtual control of the quadcopter system. The estimated disturbance is used directly in the passive FTC. At the same time, a modified controller structure is designed to achieve the passive FTC ability for two and three rotor failure. To avoid the control allocation switching from the fault-free control to the FTC, a dynamic control allocation is used. In addition, the closed-loop stability is analyzed in the presence of up to three rotor failure. To validate the proposed uniform passive FTC method, outdoor experiments are performed for the first time, which have demonstrated that the hovering quadcopter is able to recover from one rotor failure using the proposed controller and resume its mission even if two adjacent, two opposite, or three rotors fail, without the need for any rotor fault information or controller switching.

Index Terms—Fault tolerant control, UAVs, nonlinear control systems, reliable flight control, disturbance estimation, ADA control.

Video: https://youtu.be/hmZZoT9rPFs
Code: https://github.com/RflyBUAA/DegradedControl.git

I. Introduction

In past years, the safety issue of quadcopters has gained more attention with the widespread application of the quadcopter. Fault-tolerant control (FTC) is used to improve the safety of quadcopters subject to rotor failure without further peripherals, which are essential for micro-quadcopters. The goal of FTC methods is to maintain the same functionalities in the system even if reduced performances are incurred. Both the active (e.g., [1], [2]) and passive (e.g., [3]–[7]) FTC techniques have been used to deal with quadcopter rotor fault. In an active FTC scheme, information from the monitoring unit is utilized to perform fault detection and diagnosis (FDD). The control of faulty multicopters exhibits extraordinary demand for the rotor fault information, which is then used in control algorithm reconfiguration and redundancy management to guarantee safety under design basis faults. The research for active FTC can be categorized into three main areas [8], i.e., FDD, re-configurable control, and the integration of the two. i) The FDD plays an essential role in providing fault information. However, it also imposes a severe computation burden and brings in an FDD delay, degrading system safety [9], [10]. ii) In terms of re-configurable control, it is often assumed that the faulty system is controllable as well as the original system with the same sets of controllable states identified. For quadcopters, some studies focus on the situation of partial rotor faults (e.g., [2]–[6]). Others look into the situation of complete rotor faults. For example, such as [9]–[23], authors assume that the exact fault information is known prior such that obtaining rotor fault information is saved. iii) For multicopters equipped with the integration of FDD and re-configurable control, after the rotor fault occurs, the unobservable rotor fault information [24], and the time consumption caused by the process of FDD may lead to failure in FTC especially when the fault in rotors makes the system uncontrollable.

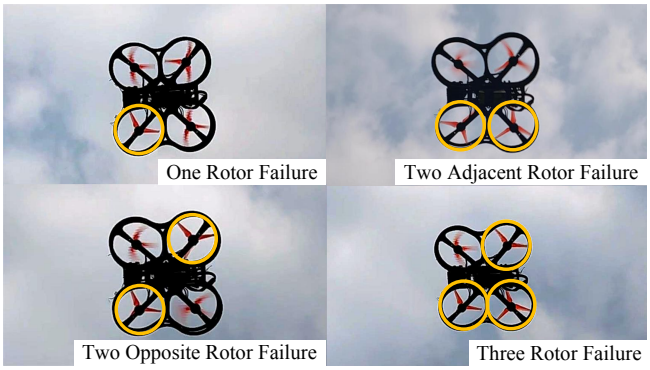

Fig. 1. Snapshots of a quadcopter with one, two adjacent, two opposite, and three rotor failure. Faulty rotors are marked out in yellow circles.

Meanwhile, passive FTC is regarded a complementary of active FTC due to its capability in avoiding above limitations. Passive fault-tolerant systems do not alter the control structure [8], considering normal conditions and design basis faults. Typically, the system redundancy has already been considered in the controller design, so there is no need to perform additional real-time management of redundancies. However, there is little research conducted on the traditional passive FTC for the quadcopter with complete rotor failure, such as in [7], due to its conservativeness.

The existing achievements about the active FTC of the quadcopter provide some foundations for achieving a uniform passive FTC in this paper. Reference [11] is the first one to give up the control of the yaw channel to achieve the control of the quadcopter with one rotor

failure. References [12], [13] show the controllability of the quadcopter with one, two, or three rotor failure with the yaw channel states given up. In addition, the term "primary axis" is introduced in [12]–[15] to separate the tilt angle control from the yaw angle control, which facilitates stability analysis and the FTC controller design with rotor failure. In [9], [22], [25], dynamic control allocation strategy is used to avoid the switching in control allocation method between the scenarios with and without rotor failures. However, it is noted that rotor fault information is needed to realize dynamic control allocation therein. Validation of proposed FTC methods under laboratory conditions are discussed in some literature, such as [10], [12]–[14]. Authors of [15], [16], [22] validate their FTC methods through outdoor experiments.

In this paper, a uniform passive FTC method for quadcopters under multiple rotor failures is proposed, with which limitations in the performance of the passive FTC are relaxed. Three important features of uniform passive FTC are worth emphasizing in the following.

1) With the uniform passive FTC method, control of quadcopters with one, two, or three rotor failure can be achieved using exactly the same controller, namely that with the same structure and parameters. This study explores the potentiality of the passive FTC method with rotor failures. The proposed controller is called the uniform as the demand for different fault-tolerant controllers for different rotor failure scenarios is exempted, and the overall controller design process is simplified. Furthermore, the FTC method proposed is capable of maintaining its functionality in case of partial faults in the rotors.
2) The proposed uniform passive FTC method for the quadcopter does not rely on result of FDD in rotors or explicit fault information as control allocation switching methods do. In this study, the rotor failure is modeled as a lumped disturbance, similar to [26]–[28], and the estimated disturbance is adopted by the uniform passive FTC, which circumvents problems incurred by the process of obtaining explicit fault information of each rotor. However, the stability subject to two or three rotor failure cannot be guaranteed if complete compensation for the lumped disturbance is performed (see Remark 5 in Section III-D). Therefore, partial compensation of the lumped disturbance (see Section IV-A) is performed in order to ensure the stability of quadcopters with multiple rotor failures, which is achieved by introducing the feedback of the desired rotor thrust.
3) The uniform passive FTC method does not rely on accurate quadcopter model parameters or the equilibrium condition calculation, which facilitates its application in practice and avoids the need for frequent adjustments of controller parameters while quadcopter parameters change.

TABLE I
Characteristics of proposed method

	Proposed Method
1	When one rotor failure, enter into a steady state without controller switching
2	A lumped disturbance estimated and then compensated for to reduce the model dependence.
3	Eliminates the requirement for the exact rotor failure information
4	No equilibrium solutions are derived in advance

Mueller and D'Andrea [13] first demonstrated on the feasibility of controlling a quadcopter with up to three rotor failure by a "feedforward + feedback" scheme, where the feedforward is derived by solving for the equilibrium with rotor failure information obtained in advance. As a result, FDD and controller switching are necessary between different scenarios in terms of multiple rotor failures. So the method represented in [13] is a switching and active FTC method. What is more, their work presents the flights of a quadcopter suffering one and two opposite rotor failure under laboratory conditions by using a motion capture system [29]. Furthermore, by using a motion capture system, a single-rotor flying vehicle and relevant experimental results are presented in [30]. These works are impressive and pioneering. However, there is still a big gap in practicality due to model uncertainties, onboard estimation uncertainties, and unsatisfactory real-time performance of FDD. To the best of our knowledge, the flights of a quadcopter subject to one, two adjacent, two opposite, and three rotor failure are presented in outdoor experiments for the first time only using GPS and onboard inertial measurement unit (IMU). The positioning accuracy and information update frequency (5Hz-10Hz) of ordinary GPS are much lower than those of indoor motion capture systems, such as VICON and OptiTrack. In addition, the indoor motion capture system provides more accurate attitude information than onboard IMU does. These imply that an outdoor experiment requires a fault-tolerant controller with much stronger robustness. In outdoor scenarios rather than laboratory environment, we demonstrate that using the proposed uniform and passive method, a quadcopter is able to recover from one rotor failure and resume its mission even if there are up to three rotor failure. Features of the proposed method are listed in Tab. I as a comparison with [13].

II. Problem Formulation

A. Modeling

The right-handed coordinate systems are adopted for the body frame and the Earth frame. The body frame axes $\{x_\mathrm{b}, y_\mathrm{b}, z_\mathrm{b}\}$ point forward, rightward, and downward, respectively. The origin of the body frame is located at the center of mass of a quadcopter. The Earth frame axes $\{x_\mathrm{e}, y_\mathrm{e}, z_\mathrm{e}\}$ point north, east, and downward to gravity, respectively. Then the model of a quadcopter is given as

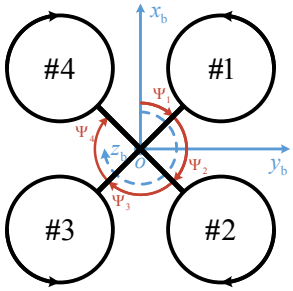

Fig. 2. Definition of rotor index and direction, and the body frame following the right-handed rule.

$$\begin{bmatrix}\dot{\mathbf{p}}\\ \dot{\mathbf{v}}\\ \dot{\mathbf{n}}_3\\ \dot{\boldsymbol{\omega}}\end{bmatrix} = \begin{bmatrix}\mathbf{v}\\ \mathbf{g}\\ -\mathbf{n}_3\times\mathbf{R}_{\mathrm{eb}}\boldsymbol{\omega}\\ \mathbf{J}^{-1}(-\boldsymbol{\omega}\times\mathbf{J}\boldsymbol{\omega})\end{bmatrix} + \begin{bmatrix}0 & 0\\ -\frac{1}{m}\mathbf{n}_3 & 0\\ 0 & 0\\ 0 & \mathbf{J}^{-1}\end{bmatrix} \underbrace{\begin{bmatrix}f\\ \boldsymbol{\tau}\end{bmatrix}}_{\mathbf{u}}, \quad (1)$$

where $\mathbf{p}\in\mathbb{R}^3$ and $\mathbf{v}\triangleq[v_x\ v_y\ v_z]^{\mathrm{T}}$ are the position and velocity of the quadcopter, respectively; $\mathbf{n}_3\triangleq\mathbf{R}_{\mathrm{eb}}\mathbf{b}_3\triangleq[n_{3,x}\ n_{3,y}\ n_{3,z}]^{\mathrm{T}}$ is the primary axis fixed on the body frame but represented in the Earth frame, $\mathbf{b}_3=[0\ 0\ 1]^{\mathrm{T}}$ is the vector pointing to the positive direction of z-axis in the body frame; $\boldsymbol{\omega}\triangleq[p\ q\ r]^{\mathrm{T}}$ is the body angular velocity; $\mathbf{g}=[0\ 0\ g]^{\mathrm{T}}$ is the vector of the gravity; m is the mass of the quadcopter; $\mathbf{R}_{\mathrm{eb}}\in\mathbb{R}^{3\times3}$ is the rotation matrix from the body frame to the Earth frame; $\mathbf{J}\triangleq\mathrm{diag}(J_x,J_y,J_z)$ is the moment of inertia of the quadcopter; $f\in\mathbb{R}_+$ and $\boldsymbol{\tau}\triangleq[\tau_p\ \tau_q\ \tau_r]^{\mathrm{T}}$ are the thrust and torque generated by rotors, respectively. In addition, $\mathbf{u}$ is called virtual control in this paper. For the quadcopter, the transformation from $\mathbf{T}$ to $\mathbf{u}$ is described as

$$\mathbf{u} = \underbrace{\begin{bmatrix}1 & 1 & 1 & 1\\ -l\sin\Psi_1 & -l\sin\Psi_2 & -l\sin\Psi_3 & -l\sin\Psi_4\\ l\cos\Psi_1 & l\cos\Psi_2 & l\cos\Psi_3 & l\cos\Psi_4\\ c & -c & c & -c\end{bmatrix}}_{\mathbf{M}}\boldsymbol{\Lambda}\mathbf{T}, \quad (2)$$

where $\mathbf{M}\in\mathbb{R}^{4\times4}$ is the control effectiveness matrix transforming $\mathbf{T}$ to $\mathbf{u}$; $\mathbf{T}\triangleq[T_1\ T_2\ T_3\ T_4]^{\mathrm{T}}$ is the desired rotor thrust vector subject to $0\leqslant T_i\leqslant T_{\max}$ and $T_{\max}\in\mathbb{R}_+$ is the maximum thrust of rotors; $l\in\mathbb{R}_+$ is the distance between the center of mass of the quadcopter and that of any of the rotors; c is the coefficient from the rotor thrust to the rotor reaction torque; $\Psi_i\in\mathbb{R}_+$ is the angle between ox_{b} and the arm of ith rotor as shown in Fig. 2; $\boldsymbol{\Lambda}=\mathrm{diag}(\lambda_1,\lambda_2,\lambda_3,\lambda_4)$ is the rotor health matrix; efficiency coefficient $\lambda_i\in[0,1]$; $\lambda_i=0$ indicates that the ith rotor is completely faulty, $\lambda_i=1$ represents that the ith rotor is fault-free; i is the index of rotors. For more information on modeling, readers can refer to [31].

B. Objective

This study supposes that the rotor health matrix $\boldsymbol{\Lambda}$ is unknown. The objective is to design a uniform passive fault-tolerant controller without control switching, and generating the desired rotor thrust vector $\mathbf{T}$ ensuring $\lim_{t\to\infty}\|\mathbf{p}(t)-\mathbf{p}_{\mathrm{d}}(t)\|=0$ when a quadcopter is fault-free or subject to rotor fault, such as $\boldsymbol{\Lambda}=\mathrm{diag}(1,1,1,1)$, $\boldsymbol{\Lambda}=\mathrm{diag}(0.5,1,1,1)$, $\boldsymbol{\Lambda}=\mathrm{diag}(0,1,1,1)$, $\boldsymbol{\Lambda}=\mathrm{diag}(0,0.7,0.6,0.8)$, $\boldsymbol{\Lambda}=\mathrm{diag}(0,0,1,1)$, $\boldsymbol{\Lambda}=\mathrm{diag}(0,1,0,1)$, and $\boldsymbol{\Lambda}=\mathrm{diag}(0,0,0,1)$.

III. Passive FTC Design

A. Outline

Since $\boldsymbol{\Lambda}$ is assumed unknown and unavailable in this paper, the disturbance caused by rotor failure is considered to lump as $\mathbf{d}$. Therefore, the virtual control $\mathbf{u}$ in (2) is rewritten as

$$\mathbf{u}=\mathbf{M}\mathbf{T}-\mathbf{d} \quad (3a)$$
$$\mathbf{d}=\mathbf{M}(\mathbf{I}_4-\boldsymbol{\Lambda})\mathbf{T}, \quad (3b)$$

where $\mathbf{M}\mathbf{T}$ is the fault-free part and $\mathbf{d}$ related to $\boldsymbol{\Lambda}$ is the lumped disturbance part. In general, the desired rotor thrust vector $\mathbf{T}$ is derived as $\mathbf{T}=\mathbf{M}^{\dagger}\mathbf{u}_{\mathrm{c}}$, which is one of control allocation strategies, where $\mathbf{M}^{\dagger}$ is Moore-Penrose inverse of $\mathbf{M}$. The control command $\mathbf{u}_{\mathrm{c}}$ is used in control allocation strategies. Furthermore, (3) becomes

$$\mathbf{u}=\mathbf{u}_{\mathrm{c}}-\mathbf{d}. \quad (4)$$

Let $\mathbf{u}_{\mathrm{c}}=\mathbf{u}_{\mathrm{d}}+\mathbf{d}$. Then, (4) becomes

$$\mathbf{u}=\mathbf{u}_{\mathrm{d}}. \quad (5)$$

Here, we will design $\mathbf{u}_{\mathrm{d}}$ to stabilize the quadcopter with one rotor failure, where $\mathbf{u}_{\mathrm{d}}$ is called the desired virtual control. However, $\mathbf{u}_{\mathrm{c}}=\mathbf{u}_{\mathrm{d}}+\mathbf{d}$ cannot be realized. On the one hand, $\mathbf{d}$ related to $\mathbf{u}_{\mathrm{c}}$ will lead to an algebraic loop. On the other hand, for a passive FTC, $\mathbf{d}$ cannot be obtained straightforwardly since $\boldsymbol{\Lambda}$ is assumed unknown. Therefore, it is desirable if the lumped disturbance $\mathbf{d}$ can be completely compensated for by letting

$$\mathbf{u}_{\mathrm{c}}=\mathbf{u}_{\mathrm{d}}+\hat{\mathbf{d}}, \quad (6)$$

where $\hat{\mathbf{d}}$ is an estimate of $\mathbf{d}$. However, the controller (6) only stabilizes the quadcopter with one rotor failure, which will be introduced in Remark 5. To achieve the passive FTC for the quadcopter with multiple rotor failures, the structure of the controller (6) is modified, by introducing the feedback of the desired rotor thrust $\mathbf{T}$, as

$$\mathbf{u}_{\mathrm{c}}=\mathbf{K}_{\mathrm{rotor}}(\mathbf{u}_{\mathrm{d}}+\hat{\mathbf{d}}-\mathbf{M}\mathbf{T}), \quad (7)$$

where $\mathbf{K}_{\mathrm{rotor}}\in\mathbb{R}^{4\times4}$ is a diagonal matrix.

Next, we will provide a detailed outline of the controller design, which is structured as follows.

1) Position Controller: To achieve position control, the position information is used to generate the desired primary axis $\mathbf{x}_{1,\mathrm{d}}\triangleq[n_{3,x,\mathrm{d}}\ n_{3,y,\mathrm{d}}]^{\mathrm{T}}$ and the desired vertical velocity $v_{z,\mathrm{d}}$.

2) Uniform Passive Fault-Tolerant Control: The uniform passive fault-tolerant controller is designed for the rotor failure cases to achieve the position control.

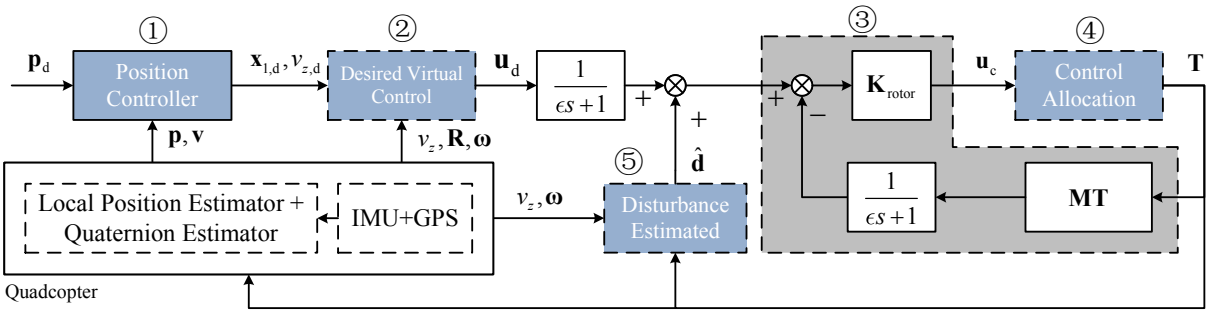

Fig. 3. The controller block scheme. Block ① corresponds to (8) and (9), block ② corresponds to (14) and (15), block ③ corresponds to (18), block ④ corresponds to (33), and block ⑤ corresponds to (12) and (13).

3) Stability Analysis: The closed-loop stability considering the estimated disturbance is shown.

4) Dynamic Control Allocation: The dynamic control allocation is introduced to avoid switching between the rotor fault-free and rotor failure cases.

B. Position Controller

Given the desired position $\mathbf{p}_\mathrm{d}$, the desired primary axis is obtained as [14]

$$\begin{aligned}\mathbf{n}_{3,\mathrm{d}} &\triangleq \begin{bmatrix}\mathbf{x}_{1,\mathrm{d}}^\mathrm{T} & n_{3,z,\mathrm{d}}\end{bmatrix}^\mathrm{T} \\ &= -(\mathbf{a}_\mathrm{d}-\mathbf{g})/\|\mathbf{a}_\mathrm{d}-\mathbf{g}\|,\end{aligned} \tag{8}$$

where

$$\begin{aligned}\mathbf{a}_\mathrm{d} &= \mathrm{sat}(\mathbf{K}_\mathbf{v}(\mathbf{v}_\mathrm{d}-\mathbf{v}), a) \\ \mathbf{v}_\mathrm{d} &= [v_{x,\mathrm{d}}\ v_{y,\mathrm{d}}\ v_{z,\mathrm{d}}]^\mathrm{T} = k_\mathrm{p}(\mathbf{p}_\mathrm{d}-\mathbf{p}),\end{aligned} \tag{9}$$

$\mathbf{K}_\mathbf{v} = \mathrm{diag}(k_v, k_v, k_{v,z}) > 0$, and the saturation function $\mathrm{sat}(\cdot)$ [31, p.233] is defined as

$$\mathrm{sat}(\mathbf{u}, a) = \begin{cases}\mathbf{u} & \|\mathbf{u}\| \leqslant a \\ \frac{a}{\|\mathbf{u}\|}\mathbf{u} & \|\mathbf{u}\| > a\end{cases}.$$

In summary, $\mathbf{x}_{1,\mathrm{d}}$ in (8) and $v_{z,\mathrm{d}}$ in (9) are designed. The position controller corresponds to ① in Fig. 3.

C. Uniform Passive Fault-Tolerant Control

The structure of the uniform passive fault-tolerant controller has been shown in (7). For severe rotor faults, such as one rotor failure, the yaw channel τ_r is uncontrollable [11] and will be given up. Under this condition, only the virtual control $\mathbf{u}_1 \triangleq [f\ \tau_p\ \tau_q]^\mathrm{T}$ is used to achieve the FTC. Therefore, the quadcopter model (1) will be decomposed first. Secondly, the lumped disturbance estimation $\hat{\mathbf{d}}$ is given. Then, $\mathbf{u}_\mathrm{d}$ composed of $\mathbf{u}_{\mathrm{d},1} = [f_\mathrm{d}\ \tau_{p,\mathrm{d}}\ \tau_{q,\mathrm{d}}]^\mathrm{T}$ and $\tau_{r,\mathrm{d}}$ is designed. At last, control command $\mathbf{u}_\mathrm{c}$ composed of $\mathbf{u}_{\mathrm{c},1} = [f_\mathrm{c}\ \tau_{p,\mathrm{c}}\ \tau_{q,\mathrm{c}}]^\mathrm{T}$ and $\tau_{r,\mathrm{c}}$ is shown in detail. Furthermore, the method to obtain $\mathbf{T}$ from $\mathbf{u}_\mathrm{c}$ will be introduced.

1) Decomposition of a quadcopter model: According to τ_r and $\mathbf{u}_1$, the quadcopter model (1) is decomposed into the yaw channel and the other. Based on (1) and (3), the model for the yaw channel on state r is

$$\begin{aligned}J_z\dot{r} &= -(J_y-J_x)pq+\tau_r \\ \tau_r &= \mathbf{E}_2\mathbf{M}\mathbf{T}-d_{\tau_r},\end{aligned} \tag{10}$$

where $d_{\tau_r} = \mathbf{E}_2\mathbf{d}$ and $\mathbf{E}_2 = [0\ 0\ 0\ 1]$. For the virtual control $\mathbf{u}_1$, the model based on the states $\mathbf{x}_2 \triangleq [v_z\ p\ q]^\mathrm{T}$ and $\mathbf{x}_1 = [n_{3,x}\ n_{3,y}]^\mathrm{T}$ will be shown. At first, define

$$\mathbf{R}_\mathrm{eb} \triangleq \begin{bmatrix}A & C & n_{3,x}\\ B & D & n_{3,y}\\ E & F & n_{3,z}\end{bmatrix} \triangleq \begin{bmatrix}\mathbf{n}_1 & \mathbf{n}_2 & \mathbf{n}_3\end{bmatrix}.$$

Then, $\dot{\mathbf{x}}_1$ is derived as

$$\begin{bmatrix}\dot{n}_{3,x}\\ \dot{n}_{3,y}\end{bmatrix} = \begin{bmatrix}-C & A\\ -D & B\end{bmatrix}\begin{bmatrix}p\\ q\end{bmatrix}$$

from the relationship $\dot{\mathbf{R}}_\mathrm{eb} = \mathbf{R}_\mathrm{eb}[\boldsymbol{\omega}]_\times$, where

$$[\boldsymbol{\omega}]_\times \triangleq \begin{bmatrix}0 & -r & q\\ r & 0 & -p\\ -q & p & 0\end{bmatrix}.$$

Then, based on (1) and (3), the quadcopter model about the states $\mathbf{x}_1$ and $\mathbf{x}_2$ is rewritten as

$$\dot{\mathbf{x}}_1 = \mathbf{A}_1\mathbf{x}_2 \tag{11a}$$

$$\dot{\mathbf{x}}_2 = \mathbf{A}_2\mathbf{x}_2+\mathbf{D}_2+\mathbf{B}_2\mathbf{u}_1 \tag{11b}$$

$$\mathbf{u}_1 = \mathbf{E}_1\mathbf{M}\mathbf{T}-\mathbf{d}_1, \tag{11c}$$

where $\mathbf{d}_1 = \mathbf{E}_1\mathbf{d}$, $\mathbf{E}_1 = [\mathbf{I}_3\ \mathbf{0}_{3\times1}]$, and

$$\mathbf{A}_1 = \begin{bmatrix}0 & -C & A\\ 0 & -D & B\end{bmatrix},$$

$$\mathbf{A}_2 = \begin{bmatrix}0 & 0 & 0\\ 0 & 0 & -\frac{J_z-J_y}{J_x}r\\ 0 & -\frac{J_x-J_z}{J_y}r & 0\end{bmatrix},$$

$$\mathbf{B}_2 = \begin{bmatrix}-\frac{n_{3,z}}{m} & 0 & 0\\ 0 & \frac{1}{J_x} & 0\\ 0 & 0 & \frac{1}{J_y}\end{bmatrix}, \mathbf{D}_2 = \begin{bmatrix}g\\ 0\\ 0\end{bmatrix}.$$

2) Lumped disturbance estimation: The way to estimate the lumped disturbance $\mathbf{d}$ is shown as below. According to (3), the lumped disturbance $\mathbf{d}$ cannot be obtained directly from (3b) because of unknown $\mathbf{\Lambda}$. Fortunately, from (10) and (11), $\mathbf{d}$ can also be expressed as

$$\begin{aligned} \mathbf{d}_1 &= \mathbf{E}_1\mathbf{M}\mathbf{T} - \mathbf{B}_2^{-1}(\dot{\mathbf{x}}_2 - \mathbf{A}_2\mathbf{x}_2 - \mathbf{D}_2) \\ d_{\tau_r} &= \mathbf{E}_2\mathbf{M}\mathbf{T} - (J_z\dot{r} + (J_y - J_x)pq), \end{aligned} \tag{12}$$

where $\dot{\mathbf{x}}_2$ and $\dot{r}$ are not directly measurable using existing sensors. Therefore, a low-pass filter is applied to (12), obtaining

$$\hat{\mathbf{d}} = \frac{1}{\epsilon s + 1}\mathbf{d}, \quad \mathbf{d} = [\mathbf{d}_1^{\mathrm{T}}\ d_{\tau_r}]^{\mathrm{T}}, \tag{13}$$

where $\epsilon > 0$ and s is the Laplace operator. The $\dot{\mathbf{x}}_2$ and $\dot{r}$ with the low-pass filter in (13) are realized as $\frac{s}{\epsilon s+1}\mathbf{x}_2(s)$ and $\frac{s}{\epsilon s+1}r(s)$, respectively. In fact, $\epsilon = 0.06$ is selected in our experiment via trial and error. The lumped disturbance estimator for $\hat{\mathbf{d}}$ corresponds to ⑤ in Fig. 3.

3) Desired virtual control: The desired virtual control $\mathbf{u}_{\mathrm{d}}$ presented in (7) will be specified. Let $\mathbf{u}_{\mathrm{d}} = [\mathbf{u}_{\mathrm{d},1}^{\mathrm{T}}\ \tau_r]^{\mathrm{T}}$. The controller $\mathbf{u}_{\mathrm{d},1}$ is designed for (11) as

$$\mathbf{u}_{\mathrm{d},1} = \mathbf{B}_2^{-1}(-\mathbf{K}_2\tilde{\mathbf{x}}_2 - \mathbf{A}_2\mathbf{x}_2 - \mathbf{D}_2 - (\mathbf{A}_1^{\mathrm{T}} - \dot{\mathbf{K}})\tilde{\mathbf{x}}_1 + \mathbf{G}_3\mathbf{x}_2), \tag{14}$$

where $\tilde{\mathbf{x}}_1 = \mathbf{x}_1 - \mathbf{x}_{1,\mathrm{d}}$, $\tilde{\mathbf{x}}_2 = \mathbf{x}_2 - \mathbf{x}_{2,\mathrm{d}}$, $\mathbf{x}_{2,\mathrm{d}} = [v_{z,\mathrm{d}}\ p_{\mathrm{d}}\ q_{\mathrm{d}}]^{\mathrm{T}} = \mathbf{K}\tilde{\mathbf{x}}_1 + [v_{z,\mathrm{d}}\ 0\ 0]^{\mathrm{T}}$, and

$$\mathbf{K} = k_{\mathbf{n}_3}\begin{bmatrix} 0 & 0 \\ -B & A \\ -D & C \end{bmatrix},\ \mathbf{K}_2 = \begin{bmatrix} k_{v,z} & 0 & 0 \\ 0 & k_{\boldsymbol{\omega}} & 0 \\ 0 & 0 & k_{\boldsymbol{\omega}} \end{bmatrix},$$

$$\mathbf{G}_3 = \begin{bmatrix} 0 & \mathbf{0} \\ \mathbf{0} & \mathbf{G} \end{bmatrix},\ \mathbf{G} = -n_{3,z}k_{\mathbf{n}_3}\mathbf{I}_2,$$

$$\dot{\mathbf{K}} = k_{\mathbf{n}_3}\begin{bmatrix} 0 & 0 \\ -\dot{B} & \dot{A} \\ -\dot{D} & \dot{C} \end{bmatrix}.$$

Note that

$$\begin{aligned} \dot{A} &= Cr - qn_{3,x} \qquad \dot{B} = Dr - qn_{3,y} \\ \dot{C} &= -Ar + pn_{3,x} \quad \dot{D} = -Br + pn_{3,y}, \end{aligned}$$

are derived from the relationship $\dot{\mathbf{R}}_{\mathrm{eb}} = \mathbf{R}_{\mathrm{eb}}[\boldsymbol{\omega}]_{\times}$.

Remark 1. Elements of the rotation matrix $\mathbf{R}_{\mathrm{eb}}$ are used directly in (14), which means that the proposed controller does not depend on an assumption of a small Euler angle as in [22].

The controller $\mathbf{u}_{\mathrm{d},1}$ is designed as (14). Then, the controller $\tau_{r,\mathrm{d}}$ is designed for (10) as

$$\tau_{r,\mathrm{d}} = -J_z k_r(r - r_{\mathrm{d}}), \tag{15}$$

where r_{d} is the desired yaw angular rate. In this paper, $r_{\mathrm{d}} = 0$ for simplicity. In conclusion, $\mathbf{u}_{\mathrm{d}} = [\mathbf{u}_{\mathrm{d},1}^{\mathrm{T}}\ \tau_{r,\mathrm{d}}]^{\mathrm{T}}$ is designed completely. The desired virtual controllers (14) and (15), corresponding to ② of Fig. 3, are shown in Fig. 4 in detail.

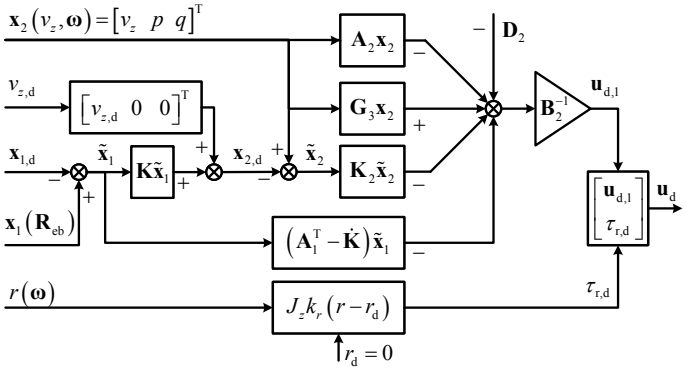

Fig. 4. The desired virtual control corresponding to ② in Fig. 3.

4) Control command: So far, the lumped disturbance estimate $\hat{\mathbf{d}}$ and the desired virtual control $\mathbf{u}_{\mathrm{d}}$ have been designed. The feedback of the desired rotor thrust $\mathbf{T}$ is introduced to ensure the stability with multiple rotor failures. The following procedures show the designation of the control command $\mathbf{u}_{\mathrm{c}}$ in detail. Based on (7), the low-pass filters are added on $\mathbf{u}_{\mathrm{d}}$ and $\mathbf{MT}$ in the following. Let $\mathbf{u}_{\mathrm{c}} = [\mathbf{u}_{\mathrm{c},1}^{\mathrm{T}}\ \tau_{r,\mathrm{c}}]^{\mathrm{T}}$. At first, $\mathbf{u}_{\mathrm{c},1}$ is designed as

$$\mathbf{u}_{\mathrm{c},1} = k_{\mathrm{rotor}}\left(\frac{1}{\epsilon s+1}\mathbf{u}_{\mathrm{d},1} + \hat{\mathbf{d}}_1 - \frac{1}{\epsilon s+1}\mathbf{E}_1\mathbf{M}\mathbf{T}\right), \tag{16}$$

where $k_{\mathrm{rotor}} > 0$. Then, $\tau_{r,\mathrm{c}}$ is designed as

$$\tau_{r,\mathrm{c}} = k_{\mathrm{rotor},z}\left(\frac{1}{\epsilon s+1}\tau_{r,\mathrm{d}} + \hat{d}_{\tau_r} - \frac{1}{\epsilon s+1}\mathbf{E}_2\mathbf{M}\mathbf{T}\right), \tag{17}$$

where $k_{\mathrm{rotor},z} > 0$. We rewrite the combination of (16) and (17) as

$$\mathbf{u}_{\mathrm{c}} = \mathbf{K}_{\mathrm{rotor}}\left(\frac{1}{\epsilon s+1}\mathbf{u}_{\mathrm{d}} + \hat{\mathbf{d}} - \frac{1}{\epsilon s+1}\mathbf{M}\mathbf{T}\right), \tag{18}$$

which corresponds to ③ in Fig. 3, where $\mathbf{K}_{\mathrm{rotor}} = \mathrm{diag}(k_{\mathrm{rotor}}, k_{\mathrm{rotor}}, k_{\mathrm{rotor}}, k_{\mathrm{rotor},z})$. With $\mathbf{u}_{\mathrm{c}}$ from (18), the Moore-Penrose inverse of $\mathbf{M}$ is directly used to obtain $\mathbf{T}$. The saturation condition of $\mathbf{T}$ will be taken into account in Section III-E. For the case of rotor failure, only $\mathbf{u}_{\mathrm{c},1}$ is necessary for the control allocation to generate $\mathbf{T}$ for the passive FTC, i.e.,

$$\mathbf{T} = (\mathbf{E}_1\mathbf{M})^{\dagger}\mathbf{u}_{\mathrm{c},1}. \tag{19}$$

Under this condition, the yaw channel is given up. The control allocation with rotor failure is realized as shown in Fig. 5(a). For the rotor fault-free case, the control command $\mathbf{u}_{\mathrm{c}}$ is used for the control allocation, i.e.,

$$\mathbf{T} = \mathbf{M}^{\dagger}\mathbf{u}_{\mathrm{c}}. \tag{20}$$

Under this condition, the yaw channel is controlled by $\tau_{r,\mathrm{c}}$. The control allocation with rotor fault-free is realized as Fig. 5(b) shows.

TABLE II
The eigenvalues of $\mathbf{N}$ for different $\mathbf{\Lambda}$

	$\mathbf{\Lambda}$	Eigenvalues of $\mathbf{N}$
One Rotor Failure	diag(0.5 1 1 1)	1 0.625 1
	diag(0 1 1 1)	1 0.25 1
	diag(0 0.7 0.6 0.8)	0.1718 0.644 0.7592
	diag(0 0.1 0.1 0.1)	0.1 0.025 0.1
Two and Three Rotor Failure	diag(0 1 0 1)	1 0 0.5
	diag(0 0.5 0 0.5)	0.5 0 0.25
	diag(1 0 1 0)	0.5 0 1
	diag(0 0 1 1)	1 0 0.5
	diag(1 1 0 0)	1 0 0.5
	diag(0 0 0 1)	0.75 0 0
	diag(0 0 1 0)	0.75 0 0

D. Stability Analysis

In Section III-C, the design of the uniform passive fault-tolerant controller is provided thoroughly. Since the lumped disturbance $\mathbf{d}$ related to $\mathbf{T}$ leads to an algebraic loop, lumped disturbance estimation $\hat{\mathbf{d}}$ is used in (18). Therefore, the closed-loop stability under rotor failure should be analyzed. The closed-loop model is obtained at first. Performing inverse Laplace transform to (16) gives us

$$\epsilon\dot{\mathbf{u}}_{\mathrm{c},1} = -\mathbf{u}_{\mathrm{c},1} + k_{\mathrm{rotor}}\left(\mathbf{u}_{\mathrm{d},1} + \mathbf{d}_1 - \mathbf{E}_1\mathbf{M}\mathbf{T}\right), \tag{21}$$

where (13) is considered. Substituting (11c) into (21) yields

$$\epsilon\dot{\mathbf{u}}_{\mathrm{c},1} = -\mathbf{u}_{\mathrm{c},1} + k_{\mathrm{rotor}}\left(\mathbf{u}_{\mathrm{d},1} - \mathbf{u}_1\right) \tag{22}$$

According to (3), (11c) is also rewritten as

$$\mathbf{u}_1 = \mathbf{E}_1\mathbf{M}\mathbf{\Lambda}\mathbf{T}. \tag{23}$$

For the case of rotor failure, substituting (19) into (23) gives us

$$\mathbf{u}_1 = \mathbf{N}\mathbf{u}_{\mathrm{c},1}, \tag{24}$$

where $\mathbf{N} = (\mathbf{E}_1\mathbf{M})\mathbf{\Lambda}(\mathbf{E}_1\mathbf{M})^{\dagger}$. Furthermore, multiply both sides of (22) by $\mathbf{N}$, (22) becomes

$$\epsilon\dot{\mathbf{u}}_1 = -(\mathbf{I}_3 + k_{\mathrm{rotor}}\mathbf{N})\mathbf{u}_1 + k_{\mathrm{rotor}}\mathbf{N}\mathbf{u}_{\mathrm{d},1} \tag{25}$$

with (24) considered, where $\mathbf{I}_3$ is introduced as the result of the feedback of the desired rotor thrust $\mathbf{T}$ and (25) is the result of the incomplete compensation for the lumped disturbance, which are discussed further in Remark 5 and Section IV-A, respectively.

Obviously, the real part of the eigenvalues of $(\mathbf{I}_3 + k_{\mathrm{rotor}}\mathbf{N})$ are always positive, even two or three rotors fail, as shown in Tab. II.

Remark 2. The real quadcopter model is used to validate the eigenvalues of $\mathbf{N}$ under different rotor fault cases. Let $l = 0.0125$, $c = 0.0166$, $\Psi_1 = \pi/4$, $\Psi_2 = 5\pi/4$, $\Psi_3 = 7\pi/4$, and $\Psi_4 = 3\pi/4$. For the given $\mathbf{\Lambda}$, the eigenvalues of $\mathbf{N}$ are listed in Tab. II.

In other words, (25) is always stable. Therefore, the closed-loop system can be depicted as

$$\begin{aligned}
\dot{\mathbf{x}}_1 &= \mathbf{A}_1\mathbf{x}_2 \\
\dot{\mathbf{x}}_2 &= \mathbf{A}_2\mathbf{x}_2 + \mathbf{D}_2 + \mathbf{B}_2\mathbf{u}_1 \\
\epsilon\dot{\mathbf{u}}_1 &= -(\mathbf{I}_3 + k_{\mathrm{rotor}}\mathbf{N})\mathbf{u}_1 + k_{\mathrm{rotor}}\mathbf{N}\mathbf{u}_{\mathrm{d},1} \\
\mathbf{u}_{\mathrm{d},1} &= \mathbf{B}_2^{-1}(-\mathbf{K}_2\tilde{\mathbf{x}}_2 - \mathbf{A}_2\mathbf{x}_2 - \mathbf{D}_2 - (\mathbf{A}_1^{\mathrm{T}} - \dot{\mathbf{K}})\tilde{\mathbf{x}}_1 + \mathbf{G}_3\mathbf{x}_2).
\end{aligned} \tag{26}$$

Theorem 1 shows the closed-loop stability of (26).

Theorem 1. Under (13), if $\mathbf{u}_1 = \mathbf{N}\mathbf{u}_{\mathrm{c},1}$ with $n_{3,z}, k_{\mathbf{n}_3}, (k_{v,z} - 0.5), (k_{\boldsymbol{\omega}} - 0.5) > 0$, then the system (26) satisfies $\|\mathbf{X}(t)\|_2 \to \mathcal{B}\left(\sqrt{\frac{\frac{1}{2}\|\mathbf{B}_2\|_2^2\|\tilde{\mathbf{u}}_1\|_2^2}{\min\left(n_{3,z}k_{\mathbf{n}_3},(k_{v,z}-0.5),(k_{\boldsymbol{\omega}}-0.5)\right)}}\right)$ as $t \to \infty$, where $\mathbf{X} = [\tilde{\mathbf{x}}_1^{\mathrm{T}}\ \tilde{\mathbf{x}}_2^{\mathrm{T}}]^{\mathrm{T}}$, $\tilde{\mathbf{u}}_1 = \mathbf{u}_1 - \mathbf{u}_{\mathrm{d},1}$.

Proof. See Appendix. □

Remark 3. This remark discusses the impact of size of ball $\mathcal{B}$ on the stability of the closed-loop system (26). Theorem 1 shows that if $\|\tilde{\mathbf{u}}_1\|_2$ is bounded, then $\|\mathbf{X}\|_2$ is uniformly ultimately bounded. Therefore, the ball $\mathcal{B}$ means that there is a steady state error around the control target, and the size of ball $\mathcal{B}$ is related to $\|\tilde{\mathbf{u}}_1\|_2$. Substituting (11c) into $\tilde{\mathbf{u}}_1$, $\tilde{\mathbf{u}}_1$ is expanded as

$$\tilde{\mathbf{u}}_1 = \mathbf{u}_1 - \mathbf{u}_{\mathrm{d},1} = \mathbf{E}_1\mathbf{M}\mathbf{T} - \mathbf{d}_1 - \mathbf{u}_{\mathrm{d},1}, \tag{27}$$

which is affected by $\mathbf{d}_1$. If the quadcopter is fault-free, $\mathbf{d}_1$ is zero in (27). When rotors fail suddenly, $\|\mathbf{d}_1\|_2 \neq 0$ and it leads to a large $\|\tilde{\mathbf{u}}_1\|_2$ than that in steady state. In other words, after rotor failing, the ball $\mathcal{B}$ in Theorem 1 will become a bigger one than that in steady state. For a hovering quadcopter ($n_{3,z} = 1 > 0, \mathbf{x}_{1,\mathrm{d}} = \mathbf{0}$), after rotor failing, the enlarged ball $\mathcal{B}$ allows $\|\tilde{\mathbf{x}}_1\|_2$ to have larger steady state error leading to $n_{3,z} \to 0$ as $\|\mathbf{x}_1\|_2^2 + n_{3,z}^2 = 1$. However, the proposed controller (14) requires $n_{3,z} > 0$ (z_b pointing to the ground). If the ball $\mathcal{B}$ is big enough such that $n_{3,z} \leqslant 0$ (z_b pointing to the sky), the proposed FTC method is unable to control the quadcopter into a steady state. In addition, when rotors fail from the fault-free condition with $r = 0$, the quadcopter is uncontrollable [13], [22]. Fortunately, when one rotor fails from the fault-free condition with $r = 0$, r can be increased to a large enough value by the three remaining rotors before $n_{3,z}$ becomes a non-positive value, which is discussed further in Remark 4 and validated by the subsequent experiment. But if multiple rotors fail simultaneously with $r = 0$, the quadcopter will lose control with $n_{3,z} \leqslant 0$ before $|r|$ becomes large enough. Therefore, the uniform passive FTC method is suitable for the situation that a large enough $|r|$ is incurred by one rotor failure and another rotor fails subsequently.

Remark 4. This remark discusses how to ensure that the passive FTC method stabilizes the quadcopter from the fault-free case to the one rotor failure case. For a spinning body, preserving the gyroscopic term $\mathbf{A}_2$ in a spinning control system helps improve closed-loop stability [32].

In [22], the degree of controllability (DOC) [33] is also introduced to analyze the improvement of the gyroscopic term $\mathbf{A}_2$ brings to the DOC. Referring to [22], [32], term $k_{\rm cp}\mathbf{A}_2\tilde{\mathbf{x}}_2$ is added on (14) to make the controller able to control the quadcopter into a steady state when one rotor fails abruptly. Then, (14) becomes

$$\begin{aligned}\mathbf{u}_{\rm d,1} = \mathbf{B}_2^{-1}(&-\mathbf{K}_2\tilde{\mathbf{x}}_2 - \mathbf{A}_2\mathbf{x}_2 - \mathbf{D}_2 \\ &- (\mathbf{A}_1^{\rm T} - \dot{\mathbf{K}})\tilde{\mathbf{x}}_1 + \mathbf{G}_3\mathbf{x}_2 + k_{\rm cp}\mathbf{A}_2\tilde{\mathbf{x}}_2),\end{aligned} \tag{28}$$

where $k_{\rm cp} > 0$. In fact, $k_{\rm cp} = 0.6$ is selected in this paper via trial and error. Obviously, the term $k_{\rm cp}\mathbf{A}_2\tilde{\mathbf{x}}_2$ does not change the stability proposed in Theorem 1. If $k_{\rm cp} = 0$, $\mathbf{u}_{\rm d,1}$ presented in (28) is also able to stabilize the quadcopter under one, two, or three rotor failure. However, with $k_{\rm cp} = 0$, $\mathbf{u}_{\rm d,1}$ presented in (28) cannot control the quadcopter into a steady state from the rotor fault-free case to the one rotor failure case.

Remark 5. This remark demonstrates that the controller structure as in (6) cannot stabilize the quadcopter under two or three rotor failure. Instead of introducing the desired rotor thrust $\mathbf{T}$ into (18), let control command $\mathbf{u}_{\rm c,1}$ become

$$\mathbf{u}_{\rm c,1} = \frac{1}{\epsilon s + 1}\mathbf{u}_{\rm d,1} + \hat{\mathbf{d}}_1 \tag{29}$$

to realize the compensation for the disturbance $\mathbf{d}_1$ presented in (11). Perform inverse Laplace transform to (29), then one has

$$\epsilon\dot{\mathbf{u}}_{\rm c,1} = -\mathbf{u}_{\rm c,1} + \mathbf{u}_{\rm d,1} + \mathbf{d}_1. \tag{30}$$

Substituting (19) into (11c), and (11c) becomes $\mathbf{u}_1 = \mathbf{u}_{\rm c,1} - \mathbf{d}_1$. Furthermore, (30) becomes

$$\epsilon\dot{\mathbf{u}}_{\rm c,1} = -\mathbf{u}_1 + \mathbf{u}_{\rm d,1}. \tag{31}$$

Then, multiply both sides of (31) by $\mathbf{N}$, and (31) becomes

$$\epsilon\dot{\mathbf{u}}_1 = -\mathbf{N}\mathbf{u}_1 + \mathbf{N}\mathbf{u}_{\rm d,1}, \tag{32}$$

with (24) considered. As shown in Tab. II, when two or three rotors fail, (32) is unstable. Therefore, the FTC under two rotor failure or three rotor failure cannot be achieved by (29).

Remark 6. Although this paper mainly discusses passive FTC under complete rotor failures, closed-loop stability of (26) should not be affected if rotors are subject to partial faults (e.g., listed in Tab. II) as shown in Theorem 1. In other words, the proposed controller is also able to achieve the FTC under partial rotor faults.

E. Dynamic Control Allocation

In Section III-C, control allocation strategies (19) and (20) are used for the rotor failure and fault-free cases, respectively. Because of the unknown rotor fault information, the switching from (20) to (19) is impracticable. To avoid the switching between (19) and (20), a dynamic control allocation strategy is adopted. As shown in Fig. 5(c), the quadratic programming based (QP-based) control allocation is adopted to obtain the desired rotor thrust vector $\mathbf{T}$ as

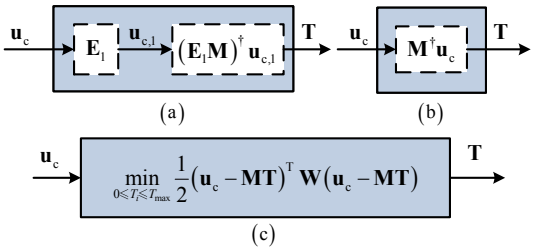

Fig. 5. The control allocation corresponding to ④ in Fig. 3: figure (a) is used for the case of rotor failure FTC, figure (b) is used for the rotor fault-free control, and figure (c) is used for both rotor failure FTC and rotor fault-free control cases.

$$\min_{0\leqslant T_i\leqslant T_{\max}} \frac{1}{2}(\mathbf{u}_{\rm c} - \mathbf{M}\mathbf{T})^{\rm T}\mathbf{W}(\mathbf{u}_{\rm c} - \mathbf{M}\mathbf{T}), \tag{33}$$

where $\mathbf{W} = {\rm diag}(w_f,\ w_{\tau_p},\ w_{\tau_q},\ w_{\tau_r})$ satisfying $w_{\tau_p} = w_{\tau_q} \gg w_f \gg w_{\tau_r} > 0$ is the weighting matrix whose diagonal elements are the weight associated with virtual control $\mathbf{u}_{\rm c}$. The control allocation method (33) corresponds to ④ in Fig. 3.

1) Influence of dynamic control allocation on the closed-loop stability: The following is the analysis of the equivalence between the control allocation strategies (20) and (33). Assuming that the constraint $0 \leqslant T_i \leqslant T_{\max}$ is not imposed, if the yaw channel can be controlled, (33) is solved for as

$$\begin{aligned}&\frac{\partial \frac{1}{2}(\mathbf{u}_{\rm c} - \mathbf{M}\mathbf{T})^{\rm T}\mathbf{W}(\mathbf{u}_{\rm c} - \mathbf{M}\mathbf{T})}{\partial \mathbf{T}} \\ &= -(\mathbf{u}_{\rm c} - \mathbf{M}\mathbf{T})^{\rm T}\mathbf{W}\mathbf{M} = 0.\end{aligned}$$

Then $\mathbf{T}$ is calculated as

$$\mathbf{T} = \underbrace{(\mathbf{M}^{\rm T}\mathbf{W}\mathbf{M})^\dagger\mathbf{M}^{\rm T}\mathbf{W}}_{\mathbf{M}^\dagger}\mathbf{u}_{\rm c} \tag{34}$$

which is consistent with (20) (see Remark 7).

The following is the analysis of the equivalence between the control allocation strategies (19) and (33). If the existing rotors cannot control the yaw channel, by setting $w_{\tau_r} = 0$, (33) is solved for as

$$\begin{aligned}&\frac{\partial \frac{1}{2}(\mathbf{u}_{\rm c,1} - \mathbf{E}_1\mathbf{M}\mathbf{T})^{\rm T}\mathbf{W}_1(\mathbf{u}_{\rm c,1} - \mathbf{E}_1\mathbf{M}\mathbf{T})}{\partial \mathbf{T}} \\ &= -(\mathbf{u}_{\rm c,1} - \mathbf{E}_1\mathbf{M}\mathbf{T})^{\rm T}\mathbf{W}_1(\mathbf{E}_1\mathbf{M}) = 0,\end{aligned}$$

where $\mathbf{W}_1 = {\rm diag}(w_f,\ w_{\tau_p},\ w_{\tau_q})$. Then $\mathbf{T}$ is calculated as

$$\mathbf{T} = \underbrace{((\mathbf{E}_1\mathbf{M})^{\rm T}\mathbf{W}_1(\mathbf{E}_1\mathbf{M}))^\dagger(\mathbf{E}_1\mathbf{M})^{\rm T}\mathbf{W}_1}_{(\mathbf{E}_1\mathbf{M})^\dagger}\mathbf{u}_{\rm c,1} \tag{35}$$

which is consistent with (19) (see Remark 7) only if $w_{\tau_r} = 0$. If w_{τ_r} satisfies $w_f \gg w_{\tau_r} \to 0$, (33) cannot be solved as (35) directly. According to the continuity of (33) about w_{τ_r}, the solution of (33) is expressed as

$$\mathbf{T} = (\mathbf{E}_1\mathbf{M})^\dagger\mathbf{u}_{\rm c,1} + \mathbf{\Delta}_{\mathbf{T}}, \tag{36}$$

where $\mathbf{\Delta_T}$ is regarded as the perturbation if $w_{\tau_r} \neq 0$. Substituting (36) into (23) yields

$$\begin{aligned}\mathbf{u}_1 &= \mathbf{E}_1\mathbf{M}\mathbf{T} - \mathbf{d}_1\\ \mathbf{d}_1 &= \mathbf{E}_1\mathbf{M}(\mathbf{I}_4 - \mathbf{\Lambda})\left((\mathbf{E}_1\mathbf{M})^\dagger\mathbf{u}_{\mathrm{c},1} + \mathbf{\Delta_T}\right).\end{aligned}$$

Therefore, $\mathbf{\Delta_T}$ will be estimated from (13) as a part of the lumped disturbance $\mathbf{d}_1$. In addition, from (36), (23) is also expressed as

$$\mathbf{u}_1 = \mathbf{N}\mathbf{u}_{\mathrm{c},1} + \mathbf{E}_1\mathbf{M}\mathbf{\Lambda}\mathbf{\Delta_T}. \tag{37}$$

We can find a $\mathbf{\Delta_N}$ satisfying $\mathbf{E}_1\mathbf{M}\mathbf{\Lambda}\mathbf{\Delta_T} = \mathbf{\Delta_N}\mathbf{u}_{\mathrm{c},1}$, where $\mathbf{\Delta_N}$ is a diagonal matrix. Then, (37) is rewritten as

$$\mathbf{u}_1 = \mathbf{N}^{'}\mathbf{u}_{\mathrm{c},1} \tag{38}$$

where $\mathbf{N}^{'} = \mathbf{N} + \mathbf{\Delta_N}$. Therefore, with (36) in consideration, (25) becomes

$$\epsilon\dot{\mathbf{u}}_1 = -(\mathbf{I}_3 + k_{\mathrm{rotor}}\mathbf{N}^{'})\mathbf{u}_1 + k_{\mathrm{rotor}}\mathbf{N}^{'}\mathbf{u}_{\mathrm{d},1}. \tag{39}$$

If the real parts of the eigenvalues of $(\mathbf{I}_3 + k_{\mathrm{rotor}}\mathbf{N}^{'})$ are always positive, the closed-loop stability under rotor failure case will not be affected by the application of dynamic control allocation scheme (33) with $w_{\tau_r} \neq 0$.

Remark 7. For (35), since $(\mathbf{E}_1\mathbf{M})^{\mathrm{T}}\mathbf{W}_1 \in \mathbb{R}^{4\times 3}$ is column full rank and $\mathbf{E}_1\mathbf{M} \in \mathbb{R}^{3\times 4}$ is row full rank, according to the method for finding the Moore-Penrose inverse using full-rank decomposition and properties of the Moore-Penrose inverse, one has

$$\begin{aligned}&((\mathbf{E}_1\mathbf{M})^{\mathrm{T}}\mathbf{W}_1(\mathbf{E}_1\mathbf{M}))^\dagger(\mathbf{E}_1\mathbf{M})^{\mathrm{T}}\mathbf{W}_1\\ =&(\mathbf{E}_1\mathbf{M})^\dagger((\mathbf{E}_1\mathbf{M})^{\mathrm{T}}\mathbf{W}_1)^\dagger(\mathbf{E}_1\mathbf{M})^{\mathrm{T}}\mathbf{W}_1\\ =&(\mathbf{E}_1\mathbf{M})^\dagger.\end{aligned}$$

In the same way, $(\mathbf{M}^{\mathrm{T}}\mathbf{W}\mathbf{M})^\dagger\mathbf{M}^{\mathrm{T}}\mathbf{W} = \mathbf{M}^\dagger$ presented in (34) also holds.

Remark 8. The attitude and position estimation errors can also be considered as a part of $\mathbf{\Delta_T}$, indicating that the proposed controller has robustness against such errors and facilitates FTC in scenarios with low precision in attitude and position estimation, especially for outdoor applications.

2) Influence of rotor saturation on the closed-loop stability: For the influence of the desired rotor thrust saturation on the closed-loop stability, the same analysis method is used. If the constraint $0 \leqslant T_i \leqslant T_{\max}$ is imposed in (33), its influence on $\mathbf{T}$ is also estimated as a part of the lumped disturbance $\mathbf{d}_1$ and leads to (39). Therefore, the saturation of desired rotor thrust vector $\mathbf{T}$ is not easy to affect the stability of the closed-loop system (26).

In conclusion, the application of the control allocation strategy (33) is equivalent to realizing adaptive and smooth "switching" between (19) and (20), without relying on the rotor fault information.

IV. Properties of Passive FTC

In this section, two properties of the passive FTC are shown.

A. Incomplete compensation for the lumped disturbance

By using (18), the lumped disturbance is not fully compensated for, which is analyzed by obtaining the static relationship between the virtual control $\mathbf{u}_1$, the desired virtual control $\mathbf{u}_{\mathrm{d},1}$, and the lumped disturbance $\mathbf{d}_1$.

Substituting (19) into (21), one has

$$\epsilon\dot{\mathbf{u}}_{\mathrm{c},1} = -\mathbf{u}_{\mathrm{c},1} + k_{\mathrm{rotor}}\left(\mathbf{u}_{\mathrm{d},1} + \mathbf{d}_1 - \mathbf{u}_{\mathrm{c},1}\right). \tag{40}$$

At the same time, from (19), (11c) becomes

$$\mathbf{u}_1 = \mathbf{u}_{\mathrm{c},1} - \mathbf{d}_1. \tag{41}$$

For (40), let $\dot{\mathbf{u}}_{\mathrm{c},1} = \mathbf{0}$, and one has

$$\mathbf{u}_{\mathrm{c},1} = \frac{k_{\mathrm{rotor}}}{k_{\mathrm{rotor}}+1}(\mathbf{u}_{\mathrm{d},1} + \mathbf{d}_1). \tag{42}$$

Then, substituting (42) into (41) yields

$$\mathbf{u}_1 = \frac{k_{\mathrm{rotor}}}{k_{\mathrm{rotor}}+1}\mathbf{u}_{\mathrm{d},1} + \frac{1}{k_{\mathrm{rotor}}+1}(-\mathbf{d}_1). \tag{43}$$

With (18), the open-loop virtual control (41) becomes (43). In other words, by introducing the feedback of the desired rotor thrust $\mathbf{T}$ in (18), the lumped disturbance is not fully compensated for, which is shown in (43). However, if the control command $\mathbf{u}_{\mathrm{c},1}$ is constructed without the desired rotor thrust $\mathbf{T}$ (see Remark 5), (30) becomes

$$\mathbf{u}_{\mathrm{c},1} = \mathbf{u}_{\mathrm{d},1} + \mathbf{d}_1 \tag{44}$$

with $\dot{\mathbf{u}}_{\mathrm{c},1} = \mathbf{0}$. Furthermore, (41) becomes

$$\mathbf{u}_1 = \mathbf{u}_{\mathrm{d},1}, \tag{45}$$

which means that the lumped disturbance is completely compensated for and the closed-loop system subject to two or three rotor failure is not stable (see Remark 5 and Tab. II).

Benefiting from the incomplete compensation for the lumped disturbance, when one rotor fails, three rather than two working rotors will be used automatically. Compared with (45), (43) includes the lumped disturbance $\mathbf{d}_1$ and the desired virtual control $\mathbf{u}_{\mathrm{d},1}$. In a physical sense, a disturbance from a faulty rotor is regarded as a counteracting force on this rotor, as shown in Fig. 6. Therefore, when one rotor fails, the quadcopter tends to tilt to the side of the faulty rotor, which is driven by the three remaining rotors.

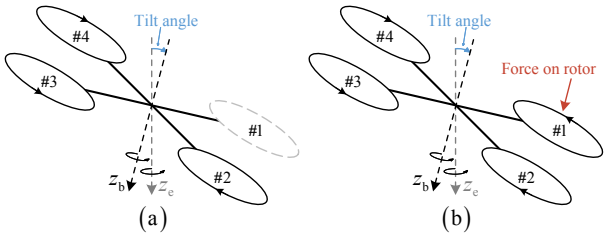

Fig. 6. When #1 rotor has a partial fault or complete failure, #3 rotor is also used to drive the quadcopter together with #2 and #4 rotors, as shown in plot (a). This is regarded as a fault-free quadcopter with a force on #1 rotor, as plotted in (b).

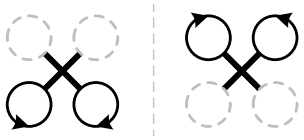

Fig. 7. Situations where a quadcopter with rotor failure cannot be stabilized by the uniform passive FTC method.

B. Ability of the uniform passive FTC

For the rotor-failure quadcopter, it is necessary to maintain $|r| \gg 0$ to achieve controllability [13], [22]. Same as in [9], [11]–[16], [22], [25], the proposed uniform passive FTC method does not actively maintain $|r| \gg 0$, but gives up the control of r. For the case of one rotor failure, the three remaining rotors will generate $\tau_r \neq 0$ leading to r with the same sign (i.e., $r\tau_r > 0$) and then ensures the controllability of the quadcopter. But the case of multiple rotor failures is a little more complicated. If the remaining rotors generate τ_r making $r\tau_r < 0$, the decreasing $|r|$ will make the quadcopter lose controllability.

Lost of control will take place in case of two rotor failure, as shown in Fig. 7. Here, the static analysis for the case of out of control is given. At first, $\mathbf{x}_{1,\mathrm{d}} = [0\ 0]^{\mathrm{T}}$ and $v_{z,\mathrm{d}} = 0$ are assumed for simplicity. Then (28) is expanded as

$$\begin{aligned}\mathbf{u}_{\mathrm{d},1} = \mathbf{B}_2^{-1}\Bigg(&- \begin{bmatrix} k_{v,z} & 0 & 0 \\ 0 & k_{\boldsymbol{\omega}} & 0 \\ 0 & 0 & k_{\boldsymbol{\omega}} \end{bmatrix} \left(\begin{bmatrix} v_z \\ p \\ q \end{bmatrix} - \underbrace{k_{\mathbf{n}_3} \begin{bmatrix} 0 \\ -F \\ E \end{bmatrix}}_{\mathbf{K}\mathbf{x}_1} \right) \\ &- \begin{bmatrix} 0 & 0 & 0 \\ 0 & 0 & -\frac{J_z - J_y}{J_x} r \\ 0 & -\frac{J_x - J_z}{J_y} r & 0 \end{bmatrix} \begin{bmatrix} v_z \\ p \\ q \end{bmatrix} - \begin{bmatrix} g \\ 0 \\ 0 \end{bmatrix} \\ &\underbrace{- n_{3,z} \begin{bmatrix} 0 \\ F \\ -E \end{bmatrix}}_{\mathbf{A}_1^{\mathrm{T}}\mathbf{x}_1} \underbrace{+ k_{\mathbf{n}_3} r \begin{bmatrix} 0 \\ E \\ F \end{bmatrix}}_{\dot{\mathbf{K}}\mathbf{x}_1} \underbrace{- n_{3,z} k_{\mathbf{n}_3} \begin{bmatrix} 0 \\ p \\ q \end{bmatrix}}_{-\mathbf{G}_3\mathbf{x}_2} \\ &+ k_{\mathrm{cp}} \begin{bmatrix} 0 & 0 & 0 \\ 0 & 0 & -\frac{J_z - J_y}{J_x} r \\ 0 & -\frac{J_x - J_z}{J_y} r & 0 \end{bmatrix} \left(\begin{bmatrix} v_z \\ p \\ q \end{bmatrix} - \underbrace{k_{\mathbf{n}_3} \begin{bmatrix} 0 \\ -F \\ E \end{bmatrix}}_{\mathbf{K}\mathbf{x}_1} \right) \Bigg), \end{aligned} \tag{46}$$

where $\mathbf{R}_{\mathrm{eb}}\mathbf{R}_{\mathrm{eb}}^{\mathrm{T}} = \mathbf{I}_3$, $\mathbf{R}_{\mathrm{eb}}^{\mathrm{T}}\mathbf{R}_{\mathrm{eb}} = \mathbf{I}_3$, $\mathbf{n}_3 = \mathbf{n}_1 \times \mathbf{n}_2$, $\mathbf{n}_1 = \mathbf{n}_2 \times \mathbf{n}_3$, $\mathbf{n}_2 = \mathbf{n}_3 \times \mathbf{n}_1$, and

$$\dot{\mathbf{R}}_{\mathrm{eb}} = \mathbf{R}_{\mathrm{eb}} \begin{bmatrix} 0 & -r & q \\ r & 0 & -p \\ -q & p & 0 \end{bmatrix}$$

are used.

Considering the initial condition ${}^{\mathrm{e}}p = {}^{\mathrm{e}}q = 0, n_{3,z}, r, {}^{\mathrm{e}}r > 0$, the body angular rate $\boldsymbol{\omega}$ is

$$\begin{bmatrix} p \\ q \\ r \end{bmatrix} = \mathbf{R}_{\mathrm{eb}}^{\mathrm{T}} \begin{bmatrix} 0 \\ 0 \\ {}^{\mathrm{e}}r \end{bmatrix} = \begin{bmatrix} E \\ F \\ n_{3,z} \end{bmatrix} {}^{\mathrm{e}}r. \tag{47}$$

Then, substituting (47) into (46), $\tau_{p,\mathrm{d}}$ and $\tau_{q,\mathrm{d}}$ are

$$\begin{aligned}\tau_{p,\mathrm{d}} = &-k_{\boldsymbol{\omega}}({}^{\mathrm{e}}rE + k_{\mathbf{n}_3}F) + \frac{J_z - J_y}{J_x} n_{3,z}\,{}^{\mathrm{e}}r^2 F - n_{3,z}F \\ &- k_{\mathrm{cp}} \frac{J_z - J_y}{J_x} n_{3,z}\,{}^{\mathrm{e}}r^2 F + k_{\mathrm{cp}} \frac{J_z - J_y}{J_x} n_{3,z}\,{}^{\mathrm{e}}r k_{\mathbf{n}_3} E \\ \tau_{q,\mathrm{d}} = &-k_{\boldsymbol{\omega}}({}^{\mathrm{e}}rF - k_{\mathbf{n}_3}E) + \frac{J_x - J_z}{J_y} n_{3,z}\,{}^{\mathrm{e}}r^2 E + n_{3,z}E \\ &- k_{\mathrm{cp}} \frac{J_x - J_z}{J_y} n_{3,z}\,{}^{\mathrm{e}}r^2 E - k_{\mathrm{cp}} \frac{J_x - J_z}{J_y} n_{3,z}\,{}^{\mathrm{e}}r k_{\mathbf{n}_3} F. \end{aligned}$$

Here, $E = -\sin\theta$ and $F = \sin\phi\cos\theta$ [31], where θ represents pitch angle and ϕ represents roll angle.

As shown in Fig. 8(a), if $\theta > 0, \phi = 0, T_1 = T_4 > 0$ and #2, #3 rotors fail, then $E < 0$ and $F = 0$. Furthermore

$$\tau_{p,\mathrm{d}} = -(k_{\boldsymbol{\omega}} - k_{\mathrm{cp}} \frac{J_z - J_y}{J_x} n_{3,z} k_{\mathbf{n}_3})\,{}^{\mathrm{e}}rE > 0$$

will make $T_4 > T_1$ (In general, the inner loop parameter $k_{\boldsymbol{\omega}}$ is larger than the outer loop parameter $k_{\mathbf{n}_3}$, and k_{cp}, $n_{3,z} < 1$ such as shown in Tab. IV). According to (2), $T_4 > T_1$ leads to $\tau_r = cT_1 - cT_4 < 0$ (with

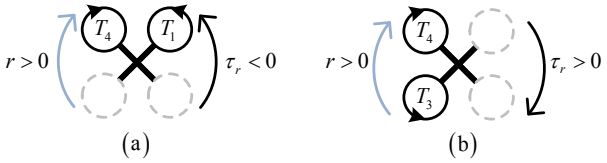

Fig. 8. In plot (a), due to $r > 0$ but $\tau_r < 0$ leading to $|r| \to 0$, then the quacopter will be uncontrollable [13], [22]. In plot (b), because of $r > 0$ and $\tau_r < 0$, then $|r|$ will be kept steady by τ_r and air damping.

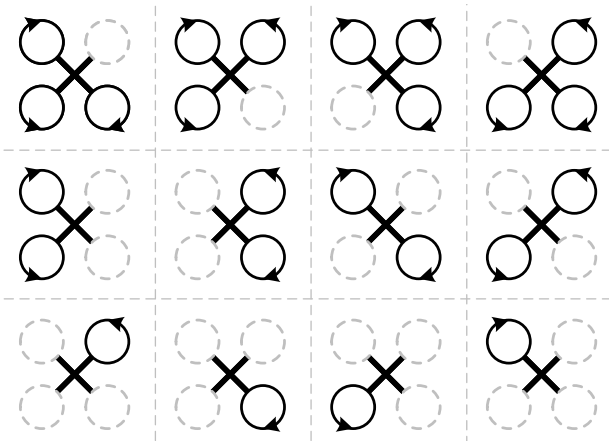

Fig. 9. Situations where a quadcopter with rotor failure will be stabilized by the uniform passive FTC method.

initial condition $r > 0$) and then $r \to 0$. However, it is important to stabilize a quadcopter with rotor failure and to keep a large enough $|r|$ to maintain controllability [13], [22]. In the same way, the situations where a quadcopter with rotor failure cannot be stabilized by the proposed uniform passive FTC are reflected in Fig. 7. Because of the unknown rotor fault information, the passive fault-tolerant controller cannot actively stop one of two remaining rotors when two adjacent rotors fail.

By contrast, as shown in Fig. 8(b), if $\theta = 0, \phi > 0, T_3 = T_4 > 0$ and #1, #2 rotors fail, then $E = 0$ and $F > 0$. Furthermore

$$\tau_{q,\mathrm{d}} = -(k_{\boldsymbol{\omega}} - k_{\mathrm{cp}} \frac{J_z - J_x}{J_y} n_{3,z} k_{\mathbf{n}_3})^{\mathrm{e}} r F < 0$$

will make $T_3 > T_4$. According to (2) and Fig. 2, $T_3 > T_4$ leads to the reaction torque $\tau_r = cT_3 - cT_4 > 0$ (with initial condition $r > 0$) then a large enough r is kept. Note that the difference between Fig. 8(a) and Fig. 8(b) is the order of rotation directions of the two remaining rotors. In Fig. 8(a), the left of the two remaining rotors is rotating clockwisely and in Fig. 8(b), the left of the two remaining rotors is rotating counterclockwisely.

Situations where quadcopters with rotor failure can be stabilized by the proposed uniform passive FTC controller are depicted in Fig. 9.

Fig. 10. The real quadcopter used in our experiments.

TABLE III
Quadcopter parameters

Parameter	Description	Values
m(kg)	Quadcopter mass	0.720
τ_{m}(s)	Rotor time constant	0.025
$T_{\max}$(N)	Rotor maximum thrust	8.5
l(m)	Arm length	0.125
$\mathbf{J}$(kg · m^2)	Moment of inertia	diag(0.0056, 0.0056, 0.0104)

V. Validation

A. Platform

The FTC method is validated in this section through the FPGA-based hardware-in-the-loop (HIL) simulation and real-flight experiments. i) The FPGA-based HIL platform is able to exchange data with the flight controller at a real-world communicate rate [34]. ii) The flight controller used in this study is Pixhawk 4 running PX4 Firmware. The Pixhawk 4 runs our control method at 400Hz with a deployment as in [35]. iii) The states of the quadcopter are obtained by the local position estimator and the complementary attitude filter (Q estimator) provided by PX4 firmware at 400Hz. The quadcopter used in experiments is shown in Fig.10. The model parameters are listed in Tab. III, where τ_{m} is the time constant of the rotor dynamics which is regarded as a first order system. Controller parameters used in the HIL simulation and real-flight experiments are listed in Tab. IV.

B. Hardware-in-the-Loop Simulations for Cases of Partial Rotor Fault

In this subsection, a suit of FPGA-based HIL simulation platform with an ARM-A53 (1.2GHz) core is adopted to validate the uniform passive FTC method under partial rotor fault. The quadcopter model runs on the simulation platform at 2kHz and interconnects with the flight controller using FPGA, which simulates real sensors, including IMU, the magnetometer, the barometer, and the GPS.

Three sets of HIL simulations are shown in Figs. 11-13. Each set includes different partial rotors fault cases, as

TABLE IV
Controller parameters

	Paramters	HIL Simulation	Experiment
Desired Primary Axis	k_{p}	0.3	0.3
	k_v	0.1	0.1
	$k_{v,z}$	1	1
	a	0.15	0.15
Desired Virtual Control	$k_{\mathbf{n}_3}$	3	3
	$k_{\boldsymbol{\omega}}$	14	14
	k_r	$0.3k_{\boldsymbol{\omega}}$	$0.3k_{\boldsymbol{\omega}}$
Control Command	ϵ	0.06	0.06
	k_{rotor}	2.0	1.3
	$k_{\mathrm{rotor},z}$	0.1	0.1
Weighting Matrix $\mathbf{W}$	w_{τ_p}, w_{τ_q}	20	20
	w_f	1	1
	w_{τ_r}	0.01	0.01

shown in the last row of each figure. When the quadcopter with faulty rotor(s) runs into a steady state, there is a rotation axis fixed to the body frame. The rotation axis is calculated as $\mathbf{n}_{\mathrm{RA}} = [n_x\ n_y\ n_z]^{\mathrm{T}} = \mathbf{R}_{\mathrm{eb}}^{\mathrm{T}}[0\ 0\ 1]^{\mathrm{T}}$, which is reached automatically rather than selected in advance [1], [12], [14]. For instance, as shown in the second row of Fig. 11, the rotation axis $\mathbf{n}_{\mathrm{RA}}$ approach stable values under different rotor fault cases. It is observed that the rotation axis $\mathbf{n}_{\mathrm{RA}}$ is determined according to different rotor fault cases rather than designed in advance. Fig. 14 shows that the quadcopter with rotor fault rotates around itself with a tilt angle corresponding to the rotation axis, which is reflected by $n_{3,z}$.

C. Experiments for Cases of Complete Rotor Failure

The uniform passive FTC under complete rotor failure cases is validated through outdoor experiments with merely GPS and onboard sensors.

To avoid the body angular rate from exceeding the single axis measurement range ($\pm 2000\,\mathrm{deg}/s$) of gyroscope ICM20689, the flight controller, i.e., Pixhawk 4, is installed on the quadcopter with a roll angle 43 deg [22]. Then, the measurable maximum angular rate around body z_{b} is about $2734\,\mathrm{deg}/s (47.7\mathrm{rad}/s)$. The experiments are divided into two parts. One is hovering flight experiments. The other one is position control experiments. Note that no rotor fault information is needed in the experiments to realize the uniform passive FTC.

1) Hovering Flight Experiments: Four hovering flight experiments in case of one, two adjacent, two opposite, and three rotor failure are shown in Fig. 16. To visually show the motion process of the primary axis $\mathbf{n}_3$, the trajectory of $\mathbf{n}_3$ is plotted on the surface of a unit sphere. When the rotor fails, the motion trajectory of the primary axis $\mathbf{n}_3$, the initial position of the primary axis (blue), and the primary axis (orange) in motion are given. At the same time, the actual moment set acting on the x_{b}-y_{b} axes after #1 rotor failure is shown in Fig. 15. The four hovering flight experiments demonstrate that the uniform passive FTC method is able to stabilize the quadcopter with one, two adjacent, two opposite, and three rotor failure by the same controller and parameters.

2) Position Control Experiments: Four position control experiments in case of one, two adjacent, two opposite, and three rotor failure are depicted as shown in Fig. 17. The desired rotor thrust and the body angular rate are also plotted. In the position control experiments, a quadcopter ran into different cases of rotor failure first. Secondly, the quadcopter followed the reference position generated by integrating the remote control channel values. The uniform passive FTC controller is able to achieve position control even if only one rotor is available.

3) Experiment Discussion: According to the desired rotor thrust of the hovering and position control experiments, while one rotor stops working, the rotor thrust will suffer saturation for a short time. Because the impact of rotor thrust saturation is considered as a part of the disturbance $\hat{\mathbf{d}}$, the uniform passive FTC controller will work properly. Obviously, for the cases of one, two adjacent, and three rotor failure, p and q have stable values, which are caused by both the angular rate ${}^{\mathrm{e}}r \neq 0$ and non-zero angle between the rotation axis and body axis z_{b}. The angular rate r in one rotor failure scenario is about 23rad/s, and that in two adjacent rotor failure scenario is about 38rad/s. The angular rate r in two opposite and three rotor failure scenarios is about 42rad/s because the whole thrust keeping current altitude is the same and generates the same reaction torque to keep the angular rate r. In the position control mode, while one rotor stops working, the quadcopter has an overshoot of less than 10 meters in the horizontal position, which is shown in Fig. 17. The quadcopter is the most capable in terms of position control if one rotor is lost. As the number of healthy rotors decreases, the controller's position control ability is reduced, as shown in Fig. 17.

Remark 9. The desired rotor thrust $\mathbf{T}$ shown in Figs. 11-13, 16, and Figs. 17 is the final control output calculated by (33). Contrary to [22], the rotor health matrix $\boldsymbol{\Lambda}$ is not used in (33). Therefore, the proposed controller will allocate a larger value to a faulty rotor than it would do if the rotor is healthy. In addition, according to (2), the actual rotor thrust vector is expressed as $\boldsymbol{\Lambda}\mathbf{T}$, which is unknown to the proposed controller.

VI. Conclusions

In this paper, we proposed a uniform passive FTC method avoiding controller and parameter switching for the quadcopter with one, two adjacent, two opposite, or three rotor failure. First, the rotor fault is modeled as a lumped disturbance acting on the virtual control, which provides four features. i) Different rotor failure conditions are stabilized by a single controller with the same set of parameters because the disturbance acting on the virtual control rather than the rotor fault information is used to design our controller. ii) In addition, the

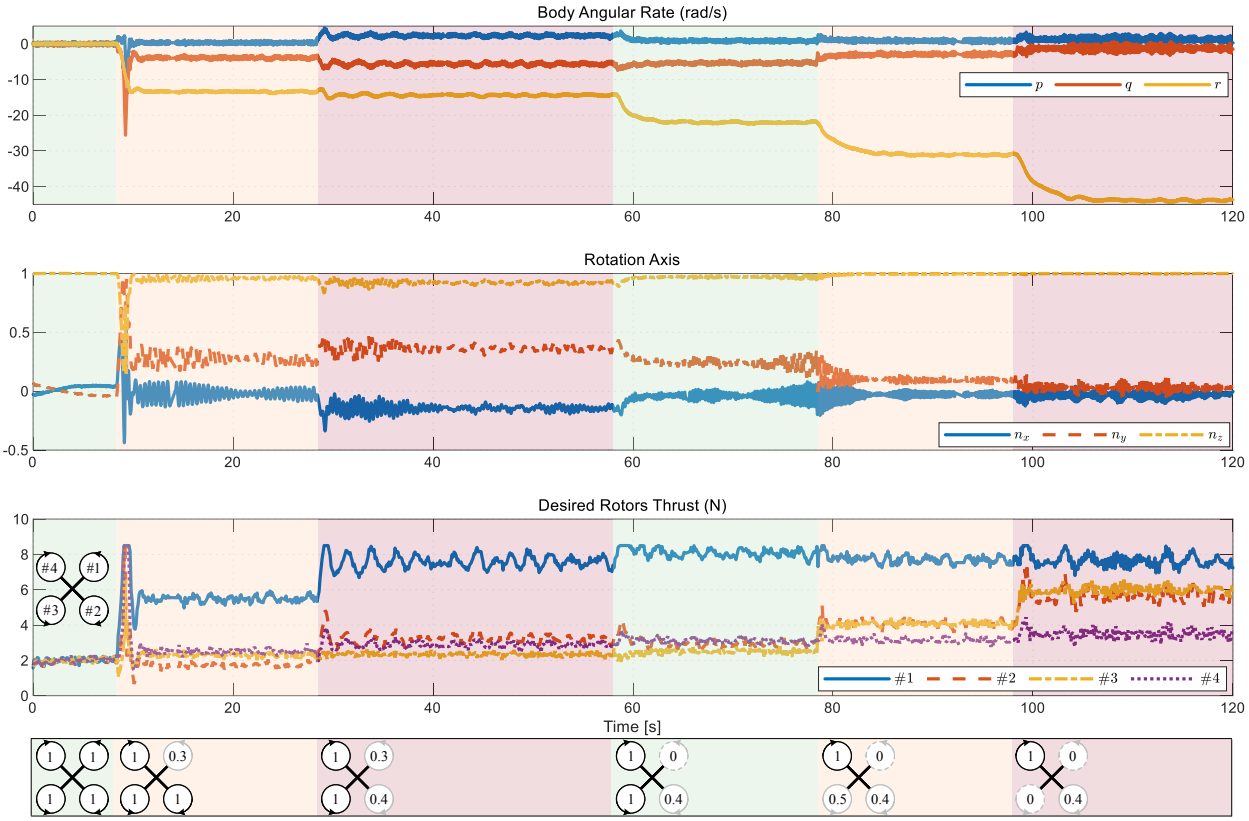

Fig. 11. HIL simulations for different partial rotor fault case. Values of efficiency coefficients of faulty rotors are marked out in the last row.

disturbance also includes the influence of the air drag torque, saturations of the rotor thrust, and perturbation of the dynamic control allocation caused by the non-zero weighting of the yaw channel. iii) The proposed method has the potential to be extended to other types of multicopters, such as hexacopters. iv) The rotation axis is automatically determined by the disturbance rather than via manual selection. Next, the uniform passive fault-tolerant controller is designed and the closed-loop stability considering the disturbance estimate is further shown. At the same time, the feedback of the desired rotor thrust is introduced to guarantee the stability of the closed-loop system subject to two and three rotor failure. Then, to avoid the switching between control allocation strategies, a dynamic control allocation scheme is adopted. Since the closed-loop stability of the FTC system relies on a large enough ${}^{\mathrm{e}}r$, two failure conditions (which are in fact equivalent), as shown in Fig. 7, cannot be stabilized by the uniform passive FTC method. Last, with only GPS and onboard sensors, the proposed controller has been validated through the HIL simulations and outdoor experiments, which indicate that the uniform passive FTC method is able to stabilize a quadcopter with one, two adjacent, two opposite, and three rotor failure and achieve the position control. The work presented in the paper is related to the emerging research direction of ADA (Autonomous, Dependable and Affordable) control [36], [37].

At last, a brief discussion on the generalization of the uniform passive FTC method for other kinds of multicopters is given. The main difference between different kinds of multicopters model is the control effectiveness matrix $\mathbf{M}$. It is used in the process of estimating disturbance $\hat{\mathbf{d}}$ instead of obtaining explicit rotors fault information. At the same time, the stability of the FTC system is independent of $\mathbf{M}$. Therefore, in theory, this method can be easily ported to other kinds of multicopters just by modifying the matrix $\mathbf{M}$, which will be validated in further work.

Appendix

System (26) is rewritten as

$$\begin{aligned}\dot{\mathbf{x}}_1 &= \mathbf{A}_1\mathbf{x}_2\\ \dot{\mathbf{x}}_2 &= \mathbf{A}_2\mathbf{x}_2 + \mathbf{D}_2 + \mathbf{B}_2(\mathbf{u}_{\mathrm{d},1} + \tilde{\mathbf{u}}_1),\end{aligned} \tag{48}$$

where $\tilde{\mathbf{u}}_1 = \mathbf{u}_1 - \mathbf{u}_{\mathrm{d},1}$. Design a Lyapunov function as $V_1 = \frac{1}{2}\tilde{\mathbf{x}}_1^{\mathrm{T}}\tilde{\mathbf{x}}_1$. Taking the derivative of V_1 along $\dot{\mathbf{x}}_1$ presented in

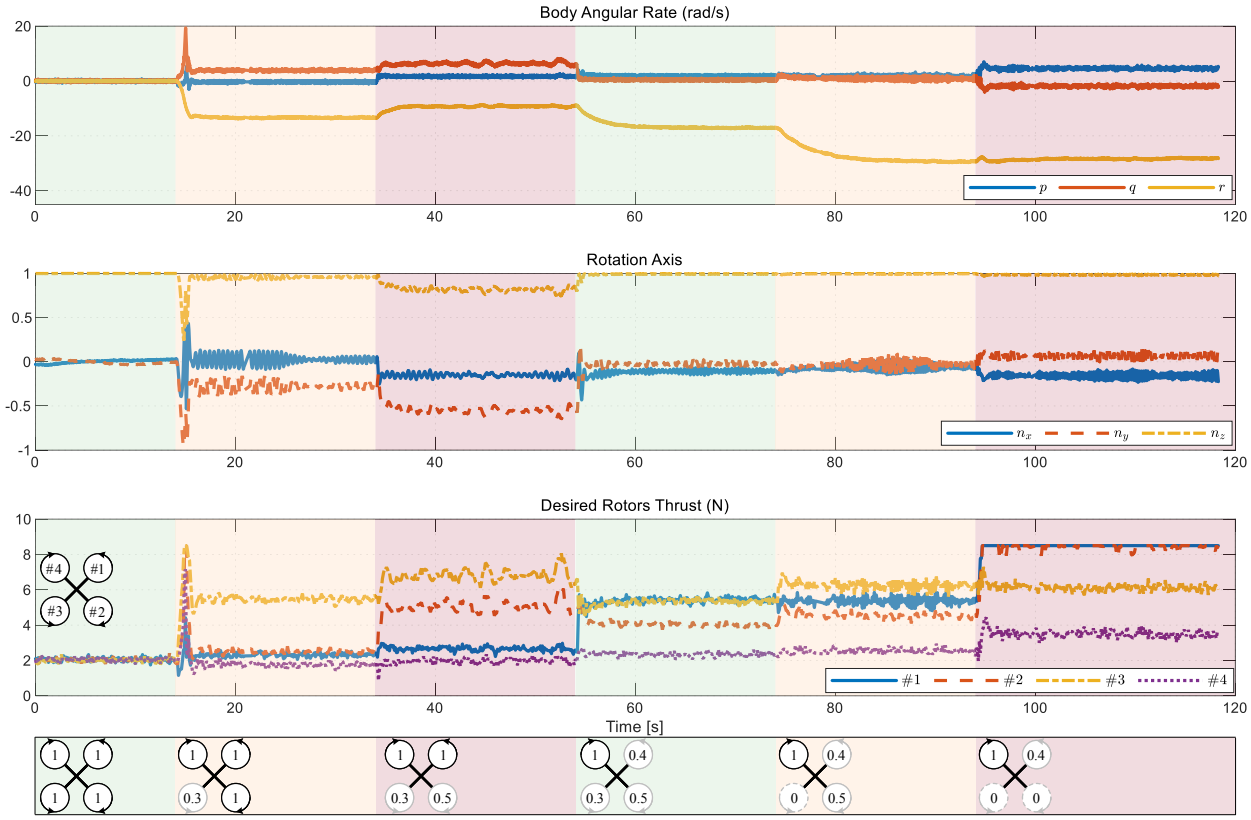

Fig. 12. HIL simulations for different partial rotor fault case. Values of efficiency coefficients of faulty rotors are marked out in the last row.

(48), one has

$$\begin{aligned}\dot{V}_1 &= \tilde{\mathbf{x}}_1^{\mathrm{T}}\dot{\mathbf{x}}_1 \\ &= \tilde{\mathbf{x}}_1^{\mathrm{T}}\mathbf{A}_1\mathbf{x}_2 \\ &= \tilde{\mathbf{x}}_1^{\mathrm{T}}\mathbf{A}_1\mathbf{x}_{2,\mathrm{d}} + \tilde{\mathbf{x}}_1^{\mathrm{T}}\mathbf{A}_1\tilde{\mathbf{x}}_2 \\ &= \tilde{\mathbf{x}}_1^{\mathrm{T}}\mathbf{A}_1\mathbf{K}\tilde{\mathbf{x}}_1 + \tilde{\mathbf{x}}_1^{\mathrm{T}}\mathbf{A}_1\tilde{\mathbf{x}}_2 + \tilde{\mathbf{x}}_1^{\mathrm{T}}\mathbf{A}_1[v_{z,\mathrm{d}}\ 0\ 0]^{\mathrm{T}} \\ &= \tilde{\mathbf{x}}_1^{\mathrm{T}}\mathbf{G}\tilde{\mathbf{x}}_1 + \tilde{\mathbf{x}}_1^{\mathrm{T}}\mathbf{A}_1\tilde{\mathbf{x}}_2,\end{aligned} \tag{49}$$

where $\mathbf{x}_{1,\mathrm{d}}$ is regarded as a constant value, $\tilde{\mathbf{x}}_1^{\mathrm{T}}\mathbf{A}_1[v_{z,\mathrm{d}}\ 0\ 0]^{\mathrm{T}} = 0$, and $\mathbf{A}_1\mathbf{K} = \mathbf{G}$ as $\mathbf{R}_{\mathrm{eb}}\mathbf{R}_{\mathrm{eb}}^{\mathrm{T}} = \mathbf{I}_3$.

Design a Lyapunov function as $V_2 = \frac{1}{2}\tilde{\mathbf{x}}_2^{\mathrm{T}}\tilde{\mathbf{x}}_2$. Taking the derivative of V_2 along $\dot{\mathbf{x}}_2$ in (48) results in

$$\begin{aligned}\dot{V}_2 &= \tilde{\mathbf{x}}_2^{\mathrm{T}}(\dot{\mathbf{x}}_2 - \dot{\mathbf{x}}_{2,\mathrm{d}}) \\ &= \tilde{\mathbf{x}}_2^{\mathrm{T}}(\mathbf{A}_2\mathbf{x}_2 + \mathbf{D}_2 + \mathbf{B}_2(\mathbf{u}_{\mathrm{d},1} + \tilde{\mathbf{u}}_1) - \dot{\mathbf{x}}_{2,\mathrm{d}}) \\ &= \tilde{\mathbf{x}}_2^{\mathrm{T}}(-\mathbf{K}_2\tilde{\mathbf{x}}_2 - \mathbf{A}_1^{\mathrm{T}}\tilde{\mathbf{x}}_1 + \mathbf{B}_2\tilde{\mathbf{u}}_1),\end{aligned} \tag{50}$$

where the controller (14) and

$$\begin{aligned}\dot{\mathbf{x}}_{2,\mathrm{d}} &= \dot{\mathbf{K}}\tilde{\mathbf{x}}_1 + \mathbf{K}\dot{\tilde{\mathbf{x}}}_1 \\ &= \dot{\mathbf{K}}\tilde{\mathbf{x}}_1 + \mathbf{K}\mathbf{A}_1\mathbf{x}_2 \\ &= \dot{\mathbf{K}}\tilde{\mathbf{x}}_1 + \mathbf{G}_3\mathbf{x}_2\end{aligned}$$

are used, $v_{z,\mathrm{d}}$ is regarded as a constant value, and $\mathbf{K}\mathbf{A}_1 = \mathbf{G}_3$ because $\mathbf{R}_{\mathrm{eb}}^{\mathrm{T}}\mathbf{R}_{\mathrm{eb}} = \mathbf{I}_3$. Define $V = V_1 + V_2 = \frac{1}{2}\mathbf{X}^{\mathrm{T}}\mathbf{X}$.

One has

$$\begin{aligned}\dot{V} &= \tilde{\mathbf{x}}_1^{\mathrm{T}}\mathbf{G}\tilde{\mathbf{x}}_1 + \tilde{\mathbf{x}}_1^{\mathrm{T}}\mathbf{A}_1\tilde{\mathbf{x}}_2 + \tilde{\mathbf{x}}_2^{\mathrm{T}}(-\mathbf{K}_2\tilde{\mathbf{x}}_2 - \mathbf{A}_1\tilde{\mathbf{x}}_1 + \mathbf{B}_2\tilde{\mathbf{u}}_1) \\ &= \tilde{\mathbf{x}}_1^{\mathrm{T}}\mathbf{G}\tilde{\mathbf{x}}_1 + \tilde{\mathbf{x}}_2^{\mathrm{T}}(-\mathbf{K}_2\tilde{\mathbf{x}}_2) + \tilde{\mathbf{x}}_2^{\mathrm{T}}\mathbf{B}_2\tilde{\mathbf{u}}_1 \\ &= \tilde{\mathbf{x}}_1^{\mathrm{T}}\mathbf{G}\tilde{\mathbf{x}}_1 - \tilde{\mathbf{x}}_2^{\mathrm{T}}\mathbf{K}_2\tilde{\mathbf{x}}_2 + \tilde{\mathbf{x}}_2^{\mathrm{T}}\mathbf{B}_2\tilde{\mathbf{u}}_1.\end{aligned} \tag{51}$$

Since the relationship

$$\begin{aligned}&\frac{1}{2}\left(\tilde{\mathbf{x}}_2 - \mathbf{B}_2\tilde{\mathbf{u}}_1\right)^{\mathrm{T}}\left(\tilde{\mathbf{x}}_2 - \mathbf{B}_2\tilde{\mathbf{u}}_1\right) \geqslant 0 \\ \Rightarrow\ &\frac{1}{2}\tilde{\mathbf{x}}_2^{\mathrm{T}}\tilde{\mathbf{x}}_2 + \frac{1}{2}\left(\mathbf{B}_2\tilde{\mathbf{u}}_1\right)^{\mathrm{T}}\left(\mathbf{B}_2\tilde{\mathbf{u}}_1\right) - \tilde{\mathbf{x}}_2^{\mathrm{T}}\mathbf{B}_2\tilde{\mathbf{u}}_1 \geqslant 0 \\ \Rightarrow\ &\frac{1}{2}\tilde{\mathbf{x}}_2^{\mathrm{T}}\tilde{\mathbf{x}}_2 + \frac{1}{2}\left(\mathbf{B}_2\tilde{\mathbf{u}}_1\right)^{\mathrm{T}}\left(\mathbf{B}_2\tilde{\mathbf{u}}_1\right) \geqslant \tilde{\mathbf{x}}_2^{\mathrm{T}}\mathbf{B}_2\tilde{\mathbf{u}}_1 \\ \Rightarrow\ &\frac{1}{2}\tilde{\mathbf{x}}_2^{\mathrm{T}}\tilde{\mathbf{x}}_2 + \frac{1}{2}\|\mathbf{B}_2\tilde{\mathbf{u}}_1\|_2^2 \geqslant \tilde{\mathbf{x}}_2^{\mathrm{T}}\mathbf{B}_2\tilde{\mathbf{u}}_1\end{aligned} \tag{52}$$

always holds, one has

$$\begin{aligned}\dot{V} &\leqslant \tilde{\mathbf{x}}_1^{\mathrm{T}}\mathbf{G}\tilde{\mathbf{x}}_1 - \tilde{\mathbf{x}}_2^{\mathrm{T}}\mathbf{K}_2\tilde{\mathbf{x}}_2 + \frac{1}{2}\tilde{\mathbf{x}}_2^{\mathrm{T}}\tilde{\mathbf{x}}_2 + \frac{1}{2}\|\mathbf{B}_2\tilde{\mathbf{u}}_1\|_2^2 \\ &= -\begin{bmatrix}\tilde{\mathbf{x}}_1 \\ \tilde{\mathbf{x}}_2\end{bmatrix}^{\mathrm{T}}\underbrace{\begin{bmatrix}n_{3,z}k_{\mathbf{n}_3}\mathbf{I}_2 & \mathbf{0} \\ \mathbf{0} & \mathbf{K}_2 - \frac{1}{2}\mathbf{I}_3\end{bmatrix}}_{\mathbf{P}_1}\begin{bmatrix}\tilde{\mathbf{x}}_1 \\ \tilde{\mathbf{x}}_2\end{bmatrix} + \frac{1}{2}\|\mathbf{B}_2\tilde{\mathbf{u}}_1\|_2^2 \\ &\leqslant -\lambda_{\min}(\mathbf{P}_1)\mathbf{X}^{\mathrm{T}}\mathbf{X} + \frac{1}{2}\|\mathbf{B}_2\tilde{\mathbf{u}}_1\|_2^2 \\ &\leqslant -\lambda_{\min}(\mathbf{P}_1)\|\mathbf{X}\|_2^2 + \frac{1}{2}\|\mathbf{B}_2\|_2^2\|\tilde{\mathbf{u}}_1\|_2^2.\end{aligned}$$

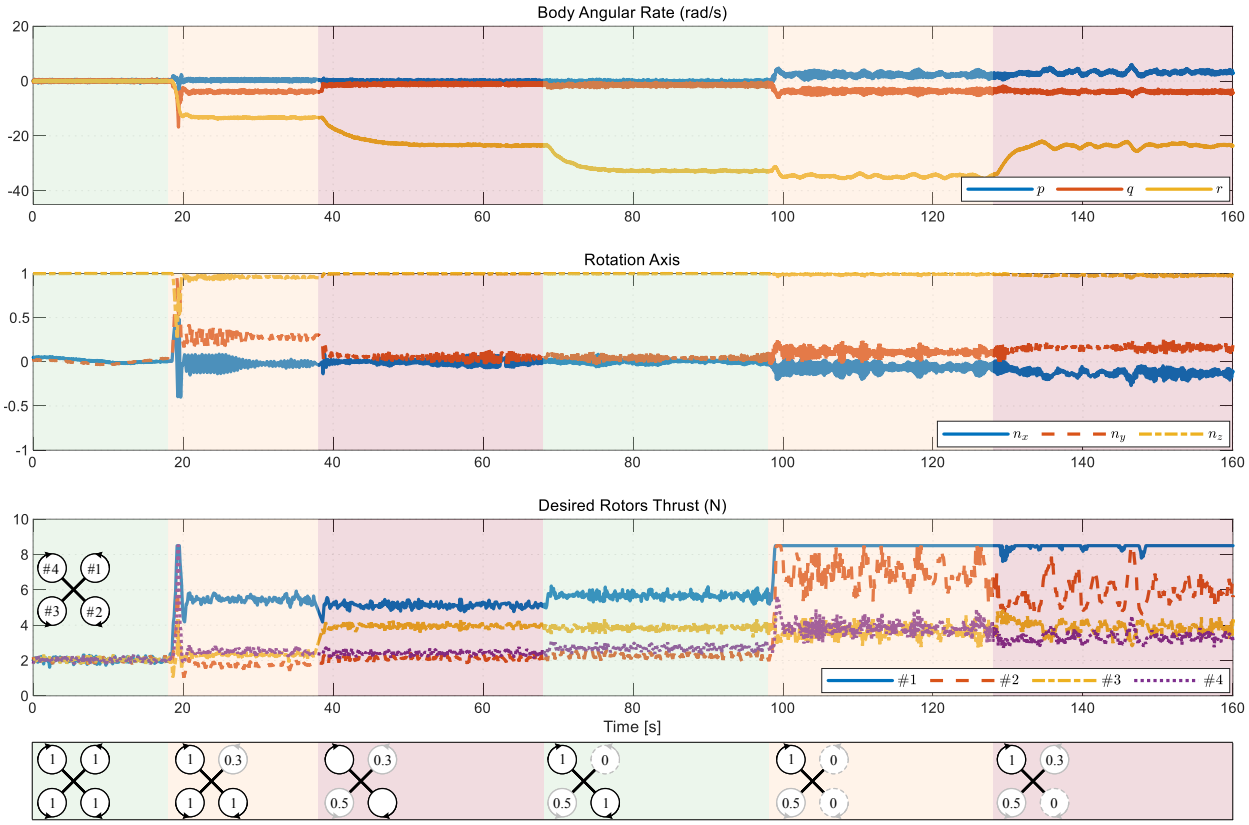

Fig. 13. HIL simulations for different partial rotor fault case. Values of efficiency coefficients of faulty rotors are marked out in the last row.

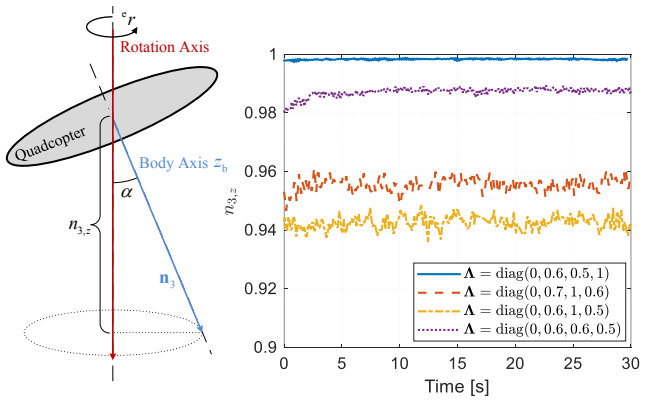

Fig. 14. Stable value of $n_{3,z}$ under different $\mathbf{\Lambda}$. Since $n_{3,z}$ is the value defined in the Earth frame, a stable $n_{3,z}$ reflects the degree of inclination of z_b against the rotation axis, namely α. It can be observed that different rotation axes are generated in case of different rotor faults.

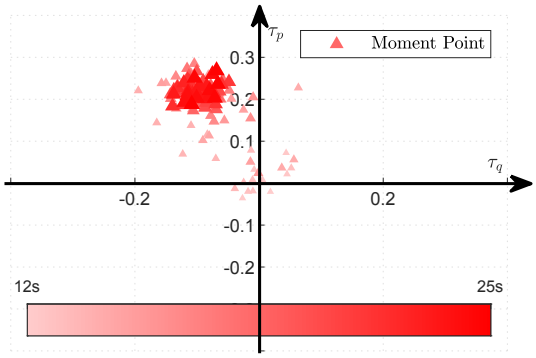

Fig. 15. Experiment: Projection of actual moment set on the τ_p-τ_q plane after one rotor failing.

Therefore, if $n_{3,z}, k_{\mathbf{n}_3}, (k_{v,z} - 0.5), (k_{\boldsymbol{\omega}} - 0.5) > 0$, then $\|\mathbf{X}(t)\|_2 \to \mathcal{B}\left(\sqrt{\frac{\frac{1}{2}\|\mathbf{B}_2\|_2^2\|\tilde{\mathbf{u}}_1\|_2^2}{\lambda_{\min}(\mathbf{P}_2)}}\right)$ as $t \to \infty$, where $\lambda_{\min}(\mathbf{P}_2) = \min\left(n_{3,z}k_{\mathbf{n}_3}, (k_{v,z} - 0.5), (k_{\boldsymbol{\omega}} - 0.5)\right)$.

References

[1] P. Lu and E. J. Van Kampen, "Active fault-tolerant control for quadrotors subjected to a complete rotor failure," IEEE International Conference on Intelligent Robots and Systems, vol. 2015-December, pp. 4698–4703, 2015.

[2] B. Wang, Y. Shen, and Y. Zhang, "Active fault-tolerant control for a quadrotor helicopter against actuator faults and model uncertainties," Aerospace Science and Technology, vol. 99, p. 105745, 2020.

[3] T. Li, Y. Zhang, and B. W. Gordon, "Passive and active nonlinear fault-tolerant control of a quadrotor unmanned aerial vehicle based on the sliding mode control technique," Proceedings of the Institution of Mechanical Engineers, Part I: Journal of Systems and Control Engineering, vol. 227, no. 1, pp. 12–23, 2012.

[4] H. Başak, E. Kemer, and E. Prempain, "A passive fault-tolerant switched control approach for linear multivariable systems: Application to a quadcopter unmanned aerial vehicle model," Journal of Dynamic Systems, Measurement, and Control, vol.

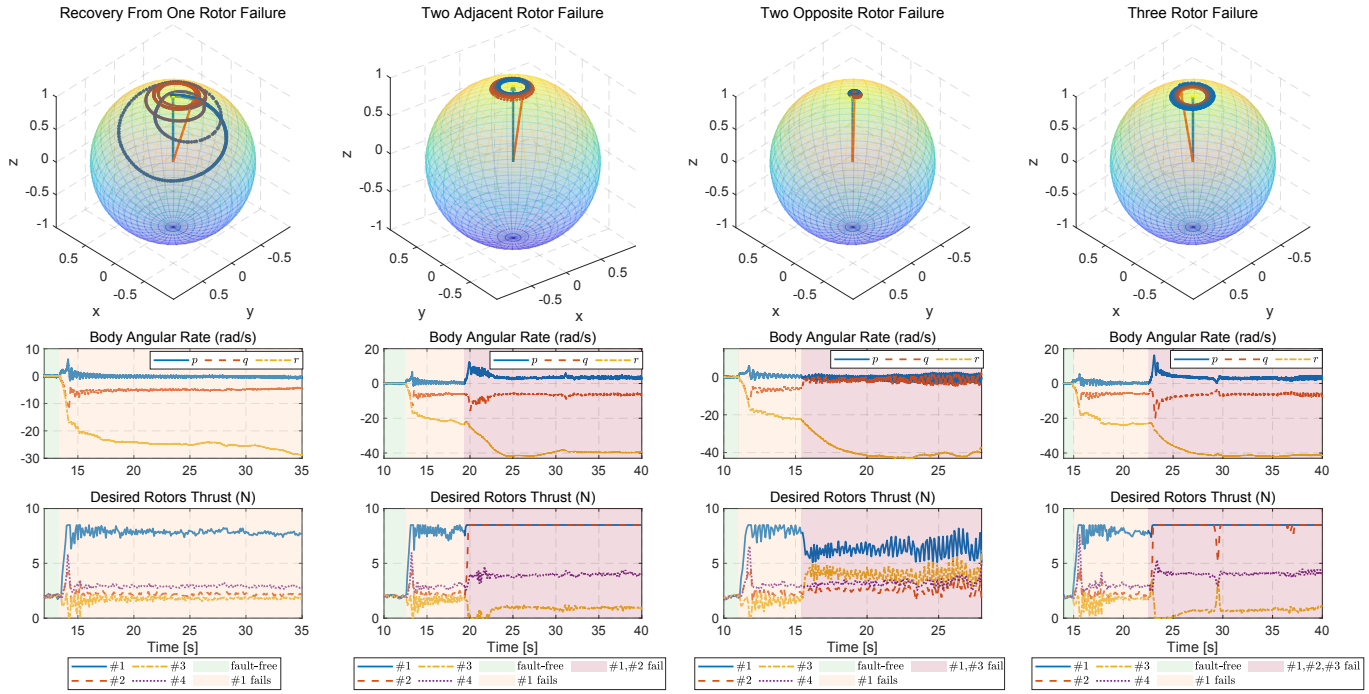

Fig. 16. Hovering Experiments: In the experiment of recovery from one rotor failure, #1 rotor of a quadcopter is stopped while the quadcopter is hovering in the sky. The quadcopter is able to recover from the failure of #1 rotor. In the experiment of two adjacent rotor failure, #1 rotor is stopped first. Secondly, the adjacent rotor (#2 rotor) is stopped. In the experiment of two opposite rotor failure, #1 rotor is stopped first. Secondly, the opposite rotor (#3 rotor) is stopped. In the experiment of three rotor failure, #1 rotor is stopped first. Secondly, #2 and #3 rotors are stopped at the same time.

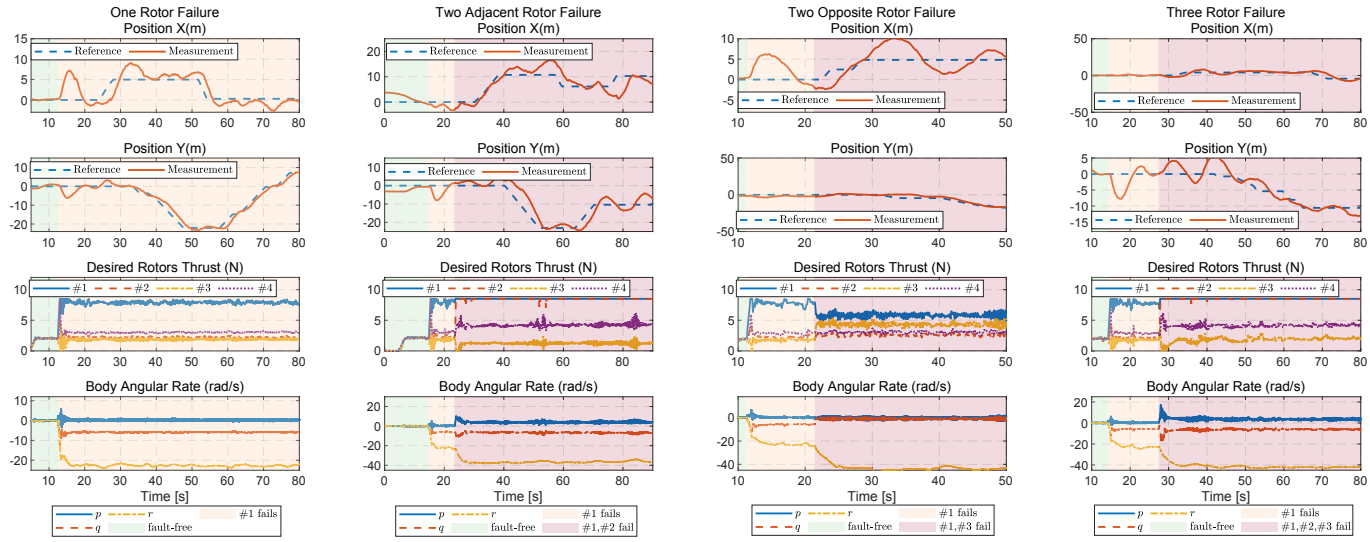

Fig. 17. Position Experiments: In the position control experiment of one rotor failure, #1 rotor is stopped. In the position control experiment of two adjacent rotor failure, #1 and #2 rotors are stopped. In the position control experiment of two opposite rotor failure, #1 and #3 rotors are stopped. In the position control experiment of three rotor failure, #1, #2, and #3 rotors are stopped.

142, no. 3, 2019.
[5] X. Zhang, Y. Zhang, C.-Y. Su, and Y. Feng, Fault-Tolerant Control for Quadrotor UAV via Backstepping Approach. American Institute of Aeronautics and Astronautics, Jan. 2010.
[6] A.-R. Merheb, H. Noura, and F. Bateman, "Design of passive fault-tolerant controllers of a quadrotor based on sliding mode theory," International Journal of Applied Mathematics and Computer Science, vol. 25, no. 3, pp. 561–576, 2015.
[7] W. Jung and H. Bang, "Fault and failure tolerant model predictive control of quadrotor UAV," International Journal of Aeronautical and Space Sciences, vol. 22, no. 3, pp. 663–675, 2021.
[8] Y. Zhang and J. Jiang, "Bibliographical review on reconfigurable fault-tolerant control systems," Annual Reviews in Control, vol. 32, no. 2, pp. 229–252, 2008.
[9] S. Sun, M. Baert, B. S. van Schijndel, and C. de Visser, "Upset recovery control for quadrotors subjected to a complete rotor failure from large initial disturbances," in 2020 IEEE

International Conference on Robotics and Automation (ICRA), 2020.

[10] F. Nan, S. Sun, P. Foehn, and D. Scaramuzza, "Nonlinear mpc for quadrotor fault-tolerant control," IEEE Robotics and Automation Letters, vol. 7, no. 2, pp. 5047–5054, 2022.

[11] A. Lanzon, A. Freddi, and S. Longhi, "Flight control of a quadrotor vehicle subsequent to a rotor failure," Journal of Guidance, Control, and Dynamics, vol. 37, no. 2, pp. 580–591, 2014.

[12] M. W. Mueller and R. D'Andrea, "Stability and control of a quadrocopter despite the complete loss of one, two, or three propellers," Proceedings - IEEE International Conference on Robotics and Automation, pp. 45–52, 2014.

[13] M. W. Mueller and R. D'Andrea, "Relaxed hover solutions for multicopters: Application to algorithmic redundancy and novel vehicles," The International Journal of Robotics Research, vol. 35, no. 8, pp. 873–889, 2015.

[14] S. Sun, L. Sijbers, X. Wang, and C. De Visser, "High-Speed Flight of Quadrotor Despite Loss of Single Rotor," IEEE Robotics and Automation Letters, vol. 3, no. 4, pp. 3201–3207, 2018.

[15] S. Sun, G. Cioffi, C. de Visser, and D. Scaramuzza, "Autonomous quadrotor flight despite rotor failure with onboard vision sensors: Frames vs. events," IEEE Robotics and Automation Letters, vol. 6, no. 2, pp. 580–587, 2021.

[16] J. Stephan, L. Schmitt, and W. Fichter, "Linear parameter-varying control for quadrotors in case of complete actuator loss," Journal of Guidance, Control, and Dynamics, vol. 41, no. 10, pp. 2232–2246, 2018.

[17] Y. Wu, K. Hu, X.-M. Sun, and Y. Ma, "Nonlinear control of quadrotor for fault tolerance: A total failure of one actuator," IEEE Transactions on Systems, Man, and Cybernetics: Systems, vol. 51, no. 5, pp. 2810–2820, 2021.

[18] A. Freddi, A. Lanzon, and S. Longhi, "A feedback linearization approach to fault tolerance in quadrotor vehicles," IFAC Proceedings Volumes, vol. 44, no. 1, pp. 5413–5418, 2011.

[19] V. Lippiello, F. Ruggiero, and D. Serra, "Emergency landing for a quadrotor in case of a propeller failure: A backstepping approach," in 2014 IEEE/RSJ International Conference on Intelligent Robots and Systems. IEEE, Sep. 2014, pp. 4782–4788.

[20] V. Lippiello, F. Ruggiero, and D. Serra, "Emergency landing for a quadrotor in case of a propeller failure: A PID based approach," in 2014 IEEE International Symposium on Safety, Security, and Rescue Robotics (2014). IEEE, Oct. 2014, pp. 1–7.

[21] A.-R. Merheb, H. Noura, and F. Bateman, "Emergency control of ar drone quadrotor UAV suffering a total loss of one rotor," IEEE/ASME Transactions on Mechatronics, vol. 22, no. 2, pp. 961–971, 2017.

[22] C. Ke, K.-Y. Cai, and Q. Quan, "Uniform fault-tolerant control of a quadcopter with rotor failure," IEEE/ASME Transactions on Mechatronics, vol. 28, no. 1, pp. 507–517, 2023.

[23] S. Sun, X. Wang, Q. Chu, and C. de Visser, "Incremental nonlinear fault-tolerant control of a quadrotor with complete loss of two opposing rotors," IEEE Transactions on Robotics, vol. 37, no. 1, pp. 116–130, 2021.

[24] G.-X. Du and L. Sun, "Loss of effectiveness information observability analysis for multicopters," in 2018 3rd International Conference on Advanced Robotics and Mechatronics (ICARM), Jul. 2018, pp. 572–576.

[25] E. Smeur, D. Höppener, and C. Wagter, "Prioritized control allocation for quadrotors subject to saturation," in International Micro Air Vehicle Conference and Flight Competition 2017, Sep. 2017, pp. 37–43.

[26] F. Ruggiero, J. Cacace, H. Sadeghian, and V. Lippiello, "Passivity-based control of VToL UAVs with a momentum-based estimator of external wrench and unmodeled dynamics," Robotics and Autonomous Systems, vol. 72, pp. 139–151, 2015.

[27] T. Tomić, C. Ott, and S. Haddadin, "External wrench estimation, collision detection, and reflex reaction for flying robots," IEEE Transactions on Robotics, vol. 33, no. 6, pp. 1467–1482, 2017.

[28] Q. Quan, G.-X. Du, and K.-Y. Cai, "Proportional-integral stabilizing control of a class of mimo systems subject to nonparametric uncertainties by additive-state-decomposition dynamic inversion design," IEEE/ASME Transactions on Mechatronics, vol. 21, no. 2, pp. 1092–1101, 2016.

[29] S. Lupashin, A. Schöllig, M. Hehn, and R. D'Andrea, "The flying machine arena as of 2010," in 2011 IEEE International Conference on Robotics and Automation, 2011, pp. 2970–2971.

[30] W. Zhang, M. W. Mueller, and R. D'Andrea, "Design, modeling and control of a flying vehicle with a single moving part that can be positioned anywhere in space," Mechatronics, vol. 61, pp. 117–130, 2019.

[31] Q. Quan, Introduction to Multicopter Design and Control. Springer Singapore, Jan. 2017.

[32] N. Raj, L. J. Colombo, and A. Simha, "Structure preserving reduced attitude control of gyroscopes," Automatica, vol. 125, p. 109471, 2021.

[33] G.-X. Du, Q. Quan, B. Yang, and K.-Y. Cai, "Controllability analysis for multirotor helicopter rotor degradation and failure," Journal of Guidance, Control, and Dynamics, vol. 38, no. 5, pp. 978–984, 2015.

[34] X. Dai, C. Ke, Q. Quan, and K.-Y. Cai, "RFlySim: Automatic test platform for UAV autopilot systems with FPGA-based hardware-in-the-loop simulations," Aerospace Science and Technology, vol. 114, p. 106727, 2021.

[35] S. Wang, X. Dai, C. Ke, and Q. Quan, "RflySim: A rapid multicopter development platform for education and research based on pixhawk and MATLAB," in 2021 International Conference on Unmanned Aircraft Systems (ICUAS). IEEE, Jun. 2021.

[36] K.-Y. Cai, K. S. Trivedi, and B. Yin, "S-ADA: Software as an autonomous, dependable and affordable system," in 2021 51st Annual IEEE/IFIP International Conference on Dependable Systems and Networks - Supplemental Volume (DSN-S), 2021, pp. 17–18.

[37] Q. Quan, G. Cui, Z. Zhao, X. Dai, C. Wen, and K.-Y. Cai, "Speculative views on health assessment of complex systems," Journal of Jilin University (Engineering and Technology Edition), vol. 53, no. 3, pp. 601–628, 2023.